Climate
of the Past

Tracing winter temperatures over the last two millennia using a north-east Atlantic coastal record

Irina Polovodova Asteman[1,2], **Helena L. Filipsson**[3], **and Kjell Nordberg**[1]

[1]Department of Marine Sciences, University of Gothenburg, Carl Skottsbergsgata 22B,
41319 Gothenburg, Sweden
[2]Currently at: Marin Mätteknik (MMT) Sweden AB, Sven Källfelts Gata 11,
42671, Gothenburg, Sweden
[3]Department of Geology, University of Lund, Sölvegatan 12, 22362 Lund, Sweden

Correspondence: Kjell Nordberg (kjell.nordberg@marine.gu.se)

Abstract. We present 2500 years of reconstructed bottom water temperatures (BWT) using a fjord sediment archive from the north-east Atlantic region. The BWT represent winter conditions due to the fjord hydrography and the associated timing and frequency of bottom water renewals. The study is based on a ca. 8 m long sediment core from Gullmar Fjord (Sweden), which was dated by ^{210}Pb and AMS ^{14}C and analysed for stable oxygen isotopes (δ^{18}O) measured on shallow infaunal benthic foraminiferal species *Cassidulina laevigata* d'Orbigny 1826. The BWT, calculated using the palaeotemperature equation from McCorkle et al. (1997), range between 2.7 and 7.8 °C and are within the annual temperature variability that has been instrumentally recorded in the deep fjord basin since the 1890s. The record demonstrates a warming during the Roman Warm Period ($\sim$ 350 BCE–450 CE), variable BWT during the Dark Ages ($\sim$ 450–850 CE), positive BWT anomalies during the Viking Age/Medieval Climate Anomaly ($\sim$ 850–1350 CE) and a long-term cooling with distinct multidecadal variability during the Little Ice Age ($\sim$ 1350–1850 CE). The fjord BWT record also picks up the contemporary warming of the 20th century (presented here until 1996), which does not stand out in the 2500-year perspective and is of the same magnitude as the Roman Warm Period and the Medieval Climate Anomaly.

1 Introduction

The climate variability over last two millennia has been widely recognized as being crucial for understanding the present and future climate responses to anthropogenic forcing (e.g. Cunningham et al., 2013; PAGES 2K, 2013; McGregor et al., 2015; Abram et al., 2016). To evaluate how significant regional climate changes are or if observed temperature anomalies are unprecedented in view of long-term climate evolution, there is a need for long historical instrumental climate records. A major challenge for the reconstructions of past climate changes, both using proxy data and utilizing paleoclimate modelling, is often a lack of such long instrumental records, which if available seldom reach beyond the 20th century. The North Atlantic region plays a paramount role in climate variability and the global carbon budget in this respect by modulating the Atlantic meridional overturning circulation (AMOC) (e.g. Eiríksson et al., 2006; Lund et al., 2006; Park and Latif, 2008; Trouet et al., 2009). The upper northern limb of the AMOC, the North Atlantic Current (Fig. 1a), delivers heat, salt and nutrients from the tropics to the mid- and high- latitudes and carries major parts of the volume flux into the Nordic Seas (Hansen and Østerhus, 2000). The AMOC is thought to be linked to the Atlantic multidecadal oscillation (AMO; Enfield et al., 2001) through sea surface temperature variability and is connected to the decadal variability of the North Atlantic Oscillation, (NAO; Curry and McCartney, 2001), where the NAO index is defined as the normalized sea level pressure difference between the Icelandic low and the Azores high (Hurrell et

al., 1995). The variability of the AMOC also contributes to a multidecadal modulation of El Niño–Southern Oscillation (ENSO) (Ortega et al., 2012 and references therein). In addition, the North Atlantic Current passes between the subpolar and subtropical gyres (Fig. 1a), from which it draws water; hence, the current depends on variability occurring within both gyres (Hansen and Østerhus, 2000). Variability of ocean temperature in the high latitude North Atlantic and Nordic Seas are reflected in the north-western European climate and in the winter Arctic sea ice extent (Årthun et al., 2017). Model projections predict that the AMOC will slowdown in response to future warming and enhanced Arctic freshwater fluxes (e.g. Schmittner et al., 2005; Ortega et al., 2012; Caesar et al., 2018) with potential impacts on the climate, ecosystems, agriculture and the economies of many European countries (e.g. Kuhlbrodt et al., 2009; Jackson et al., 2015; Knox et al., 2016). Hence, high-resolution paleoceanographic records, which preferably overlap with instrumental observations and historical data, are needed from the eastern North Atlantic region in order to document climate variability related to the physical properties of the North Atlantic Current and the AMOC strength. At the same time many of the marine records available from the region to date tend to have a low temporal resolution due to their location in the deep sea or within the open shelf areas. Sediment archives of temperate fjord inlets located within the eastern North Atlantic region offer the potential for high-resolution records of the maritime climate, because they act as sediment traps resolving climate variability at an almost annual resolution (Howe et al., 2010). Yet to date, there are relatively few such high-resolution paleoclimate records from the eastern North Atlantic fjords spanning the late Holocene (e.g. Mikalsen et al., 2001; Klitgaard-Kristensen et al., 2004; Cage and Austin, 2010; Filipsson and Nordberg, 2010; Hald et al., 2011; Kjennbakken et al., 2011; Faust et al., 2016).

Meanwhile, crucial knowledge has been gained from temperature proxy datasets available from the North Atlantic and the Northern Hemisphere in general, which represent either composite records of different climate characteristics with various temporal resolution or are a combination of historical and proxy data, and the generated data sets mostly reflect summer conditions at higher latitudes (e.g. Moberg et al., 2005; Gunnarsson et al., 2011; Butler et al., 2013; Cunningham et al., 2013; PAGES 2K, 2013, 2017; Sicre et al., 2014; Linderholm et al., 2015). In contrast, based on instrumental records, increased winter temperatures have been suggested as an important driver of the most recent warming (Cage and Austin, 2010); therefore, climate proxies incorporating winter signal are needed.

Herein, we present a bottom water temperature proxy record from the Gullmar Fjord, on the west coast of Sweden, which illustrates the climate development in north-western Europe over the last $\sim$ 2500 years. Strong advantages of the presented record in this study are its high temporal (annual to sub-decadal) resolution and the fact that a winter temperature

signal is recorded in fjord foraminiferal shells (tests) due to specific hydrographic conditions. The reconstructed temperatures are based on stable oxygen isotopes ($\delta^{18}O$) measured in tests of a shallow infaunal foraminifer *Cassidulina laevigata* d'Orbigny 1826 and reflect the deep-water temperatures in the fjord basin. The fjord has a > 100 year long record of instrumental observations from the deepest basin, performed since 1869 (Fig. 2a–c); furthermore, a > 100 year long time series of air temperature observations are also available for Stockholm, Sweden and central England. These instrumental observations of bottom water temperatures and air temperatures are used to evaluate the accuracy of the reconstructed climate variability for the last century provided by the fjord sediment archive.

2   Study area

Gullmar Fjord is a Skagerrak fjord inlet, which is 28 km long, 1–2 km wide and oriented south-west to north-east (Fig. 1). The maximum basin depth is 118.6 m. The fjord is located at a critical latitude, picking up fluctuations between cold and temperate climates, and has almost no tidal activity. The adjacent Skagerrak largely determines the local hydrography so that the deep (basin) water, which is typically exchanged in the fjord during the winter, originates from the North Sea surface water flowing into the Skagerrak with the present-day current circulation system (Svansson, 1975; Nordberg, 1991). The 42 m deep sill at the fjord entrance restricts the water exchange and results in a water column stratified due to salinity differences (Fig. 1c). At the surface (< 1 m) there is a thin layer of river water from the Örekilsälven (Fig. 1), which does not significantly impact the fjord hydrography (Arneborg, 2004). Below, at a water depth of 1–15 m, there is a brackish water mass (salinity (S) = 24–27), primarily derived from the Baltic current flowing northward along the Swedish west coast. The brackish water mass has a residence time of 20–38 days in Gullmar Fjord (Arneborg et al., 2004). A more saline water mass (S = 32–33) at $\sim$ 15–50 m is derived from the Skagerrak and has mean residence time of 29–62 days (Arneborg et al., 2004). The last and deepest layer (> 50 m), referred to herein as deep water or basin water, is more stagnant, with little seasonal or inter-annual change in salinity (ranging between 34 and 35) and an inter-annual temperature variability of 4–8 °C (Fig. 2a, b). The deep water temperatures vary between years depending on the temperature of the inflowing water mass but they remain stable seasonally (Fig. 2d). The deep-water salinities do not vary much on a seasonal basis from the average value of 34.5 (Fig. 2b). The stratification of the water column is further strengthened during the summer by the development of a strong thermocline, which impedes deep-water exchange. The deep-water exchange of the fjord basin water takes place once a year during winter, mostly between January and March, which is determined using long-term instrumental records from the
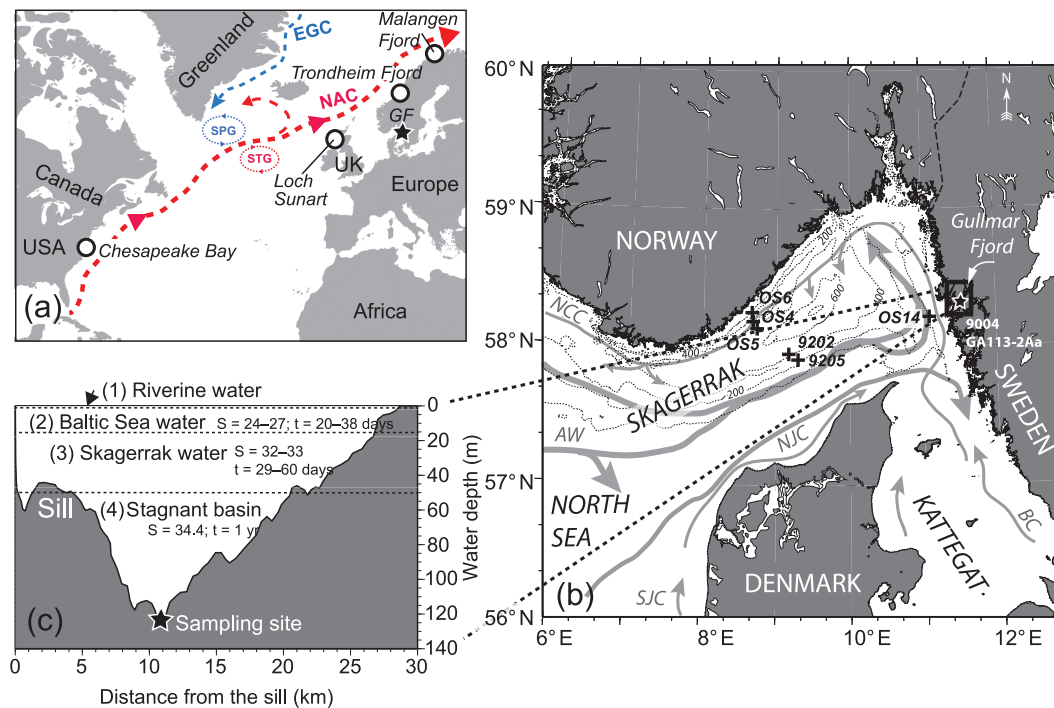
Figure 1. Map of the study area including the location of Gullmar Fjord (GF) and the sampling site for the Ga113-2Aa and 9004 records (star) within the North Atlantic **(a)** and North Sea – Skagerrak regions **(b)**. Locations of the other proxy records discussed in the text are shown by white circles, while some of the major ocean circulation characteristics mentioned in the text are indicated as follows: EGC is the East Greenland Current, NAC is the North Atlantic Current, SPG is the subpolar gyre and STG is the subtropical gyre **(a)**. **(b)** The major regional water masses and currents are shown as follows: AW is the Atlantic Water, SJC is the South Jutland Current, NJC is the North Jutland Current, BC is the Baltic Current and NCC is the Norwegian Coastal Current. **(c)** An overview of the water column stratification in the longitudinal profile of the Gullmar Fjord with an indication of the salinity (S) and residence times (t) typical for each water layer (Arneborg, 2004).

fjord (Arneborg et al., 2004). Due to the presence of a sill, isolating the fjord deep water from the adjacent sea, and the comparably large basin volume, the winter temperature and salinity of the inflowing North Sea/Skagerrak water, are "annually preserved" in the fjord basin until the next deep-water turnover the following year (Arneborg et al., 2004). This results in a deep-water environment characterized by winter temperatures. The benthic foraminifers reproduce and grow in the fjord during the spring and summer (Gustafsson and Nordberg, 2001); thus, they incorporate this annually preserved winter temperature signal of the ambient deep water into their shells. This results in a stable oxygen isotope signal mainly reflecting the winter temperatures of the North Sea surface water and the Skagerrak intermediate water flowing into the fjord during deep-water exchange.

The deep-water exchange in the fjord is driven by wind forcing, and largely depends on wind direction and wind strength (Björk and Nordberg, 2003). The latter two properties, in turn, are governed by the NAO, which is the dominant mode of climate variability in the region during the winter (Hurrell, 1995). In Gullmar Fjord, the higher frequency and duration of north-easterly winds, common during the nega-

tive NAO index periods, result in Ekman transport of surface water from the coast and facilitate coastal upwelling, which causes the deep-water exchange (Björk and Nordberg, 2003). In contrast, a positive NAO index causes prevailing westerly winds, which limit the chances of deep-water renewals occurring. From the late 1970s the NAO has been in its prolonged positive phase and is believed to be one of the triggers of severe seasonal hypoxia ($< 1 \, \mathrm{mL \, O_2}^{-1}$) in the deep fjord basin (Nordberg et al., 2000; Björk and Nordberg, 2003; Filipsson and Nordberg, 2004a).

After an extensive deep-water exchange event in the fjord the oxygen level starts to decline in June, and the lowest oxygen levels normally develop between November and January, indicating hypoxic conditions ($< 2 \, \mathrm{mL \, O_2 \, L^{-1}}$); however, so far anoxia has not been recorded (Fig. 2f). The first ever documented severe hypoxic event was noted in February 1890 by Pettersson and Ekman (1891). In the following, severe hypoxic events were measured in 1906, 1961/1962 and 1973/1974 (Fig. 2c), although due to the low observation frequency and duration of these events they are not well documented. Since 1979, multiple episodes of more frequent severe hypoxia lasting for at least 3 months have been
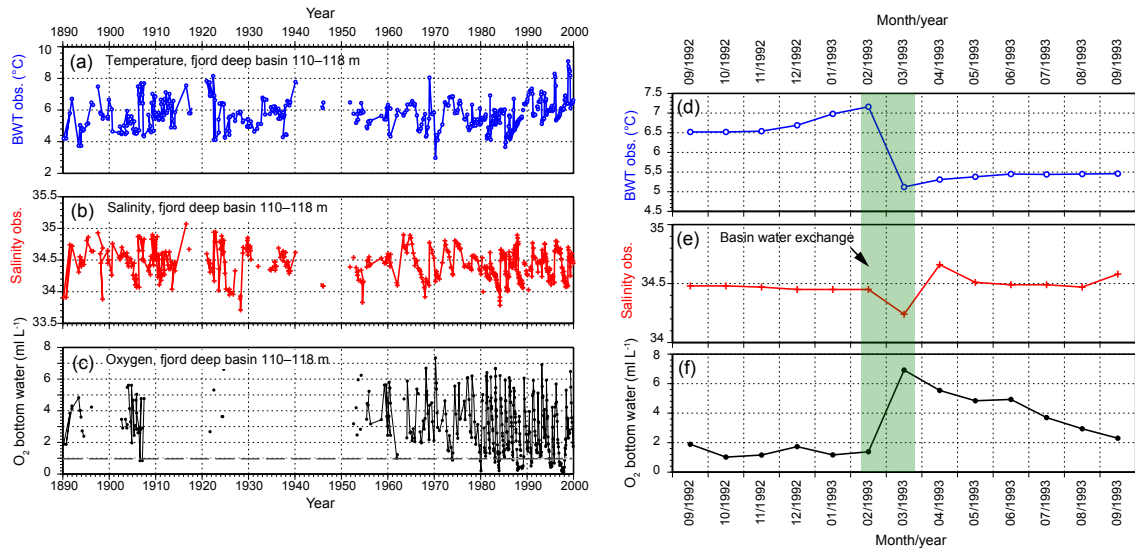
Figure 2. Hydrographic measurements from Alsbäck Deep, Gullmar Fjord taken during the 1890–2000 period below a water depth of 110 m: bottom water temperatures (BWT) **(a)**, salinity **(b)** and dissolved oxygen **(c)**. A snapshot of the hydrographic changes in BWT **(d)**, salinity **(e)** and oxygen **(f)** associated with basin water exchanges between 1992 and 1993 showing annual variability of these parameters.

observed. These events occurred in 1979/1980, 1983/1984, 1987/1988, 1988/1989, 1990/1991, 1994/1995, 1996–1998, 2008, 2014/2015 and 2016 (e.g. Filipsson and Nordberg, 2004a; Polovodova Asteman and Nordberg, 2013; SMHI SHARK-database, 2017; Nordberg et al., unpublished data).

The severe hypoxia makes the fjord basin hostile for large burrowing organisms but allows benthic meiofaunal communities to thrive. This lowers sediment bioturbation and results in a well-preserved environmental sediment archive. The fjord basin has high sediment accumulation rates, which provide a high temporal resolution corresponding to 1–6 years per 1 cm thick sediment sample. Finally, the fjord sediment archive is characterized by the diverse and abundant foraminiferal fauna and dinoflagellate cysts, which have already provided insight into climate evolution and the associated environmental changes on the Swedish west coast during the last two millennia (Filipsson and Nordberg, 2004a, 2010; Harland et al., 2006, 2013; Nordberg et al., 2009; Polovodova et al., 2011; Polovodova Asteman and Nordberg, 2013; Polovodova Asteman et al., 2013).

3   Material and methods

This study is based on a composite record of two sediment cores: GA113-2Aa and 9004. Both cores were collected at a water depth of 116 m at the same site in the deepest Gullmar Fjord basin (58°17.570′ N, 11°23.060′ E) (Fig. 1) for which the long-term hydrographic observations are available (Fig. 2a–c). Core 9004 (731 cm long) was taken with a gravity corer (⌀ = 7.6 cm) onboard R/V *Svanic* in July 1990. Core GA113-2Aa (60 cm long), which had an

intact sediment–bottom water interface, was recovered using a Gemini corer (⌀ = 8 cm) in June 1999 from the R/V *Skagerak*. In the laboratory both cores were split into two halves and sectioned at 1 cm intervals. One half was used for bulk sediment geochemistry (total carbon – TC, total nitrogen – TN and carbon to nitrogen ratio – C / N), stable oxygen and carbon isotopes, dinoflagellate cysts and benthic foraminiferal faunal analyses. Another half was stored as an archive at the Department of Geosciences, University of Gothenburg. The TC and stable carbon isotope data from both cores are published in Filipsson and Nordberg (2010), dinoflagellate cysts data are discussed in Harland et al. (2006, 2013), while C / N and foraminiferal assemblage data are presented in Filipsson and Nordberg (2004a), Polovodova et al. (2011) and Polovodova Asteman et al. (2013). We also present data from the gravity core G113-091, collected at the same location as GA113-2Aa and 9004 onboard R/V *Skagerak* in September 2009; this data is only used herein (similar to our previous study) to create a composite age model for the GA113-2Aa and 9004 cores (Polovodova Asteman et al., 2013; see below).

In addition to the above-mentioned cores, we also use six surface samples (0–1 cm) collected at five stations in the Skagerrak (OS4, OS6, OS14, 9202 and 9205) and one station in the Gullmar Fjord (G113-091a: the same location as for GA113-2Aa and 9004) in 1992–93 and 2009, respectively (Fig. 1b, c; Table 1). All surface samples were stained using Rose Bengal to distinguish individuals presumably living at the moment of sampling from the empty foraminiferal shells.
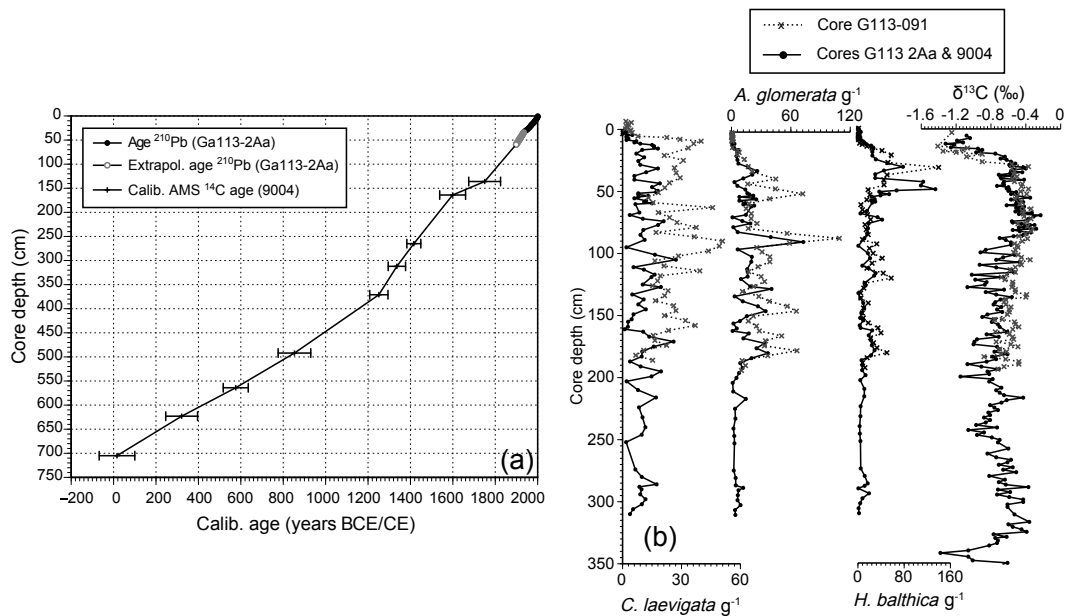
Figure 3. Age model of the studied Ga113-2Aa and 9004 records **(a)** and the comparison of foraminiferal and isotopic data with core G113-091, taken at the same location in 2009, to prove the absence of a gap between GA113-2Aa and 9004 **(b)**, according to Polovodova Asteman et al. (2013).

Table 1. Stations with collected sediment core tops and $\delta^{18}O$ analyses on living (Rose Bengal stained) *Cassidulina laevigata*.

Station	Latitude (°N)	Longitude (°E)	Water depth (m)	Sampling date (yyyy/mm/dd)	$\delta^{18}O$ (‰)
9202	57°56.2′	9°27.3′	177	1992/08/04	2.49
9202	57°56.2′	9°27.3′	177	1992/08/04	2.44
9205	57°58.4′	9°24.0′	294	1992/08/06	2.40
OS14	58°06.06′	10°58.27′	135	1993/05/09	2.58
OS4	58°18.54′	8°54.99′	325	1993/05/04	2.48
OS6	58°21.58′	8°51.01′	177	1992/08/04	2.43
G113-091	58°17.570′	11°23.060′	116	2009/09/01	2.76

3.1 Sediment core dating and age model

The age model for the composite GA113-2Aa – 9004 record was previously published in Filipsson and Nordberg (2010) with further revisions by Polovodova et al. (2011) and Polovodova Asteman et al. (2013). Eleven intact marine bivalve shells were recovered in life position from core 9004 and were subject to AMS ^{14}C analysis (Fig. 3a; Table 2). All ^{14}C dates were obtained through analysis at the Ångström Laboratory (Uppsala University, Sweden) and were originally calibrated using the marine calibration curve (Reimer et al., 2004; Bronk Ramsey, 2005). Ages were normalized to $\delta^{13}C$ of -25‰ according to Stuiver and Polach (1977), and a correction corresponding to $\delta^{13}C = 0$‰ (not measured) versus Pee Dee Belemnite (PDB) has been applied. Herein we present ages recalibrated using Calib Radiocarbon Calibration software v. 7.1 (Stuiver et al., 2017: http://calib.org/

calib/; last access: 15 March 2017), the most recent marine calibration curve (Reimer et al, 2013) and a reservoir age of 500 years ($\Delta R = 100 \pm 50$), which was obtained from pre-bomb marine bivalve shells from the Gullmar Fjord, provided by the natural history museums in Gothenburg and Stockholm (Nordberg and Posnert, unpublished data). All ages are presented as median probability with a 1-σ error margin (Table 2). Two dates at 98 and 313 cm showed minor age reversals and were omitted from the final age model (Table 2). The GA113-2Aa core was dated using ^{210}Pb and a constant rate of supply (CRS) model (Appleby and Oldfield, 1978), which suggested that the core material was deposited between ca. 1915 and 1999 (Fig. 3a). For details regarding the GA113-2Aa age model see Filipsson and Nordberg (2004a).

Together, cores GA113-2Aa and 9004 proved to be a continuous sediment record with no gap in between based

Table 2. AMS ^{14}C dates obtained for the gravity core 9004 and calibrated calendar ages. All dates presented in Filipsson and Nordberg (2010) and Polovodova Asteman et al. (2013) were re-calibrated using Calib 7.10 (Stuiver et al., 2017), the Marine13 calibration dataset (Reimer et al., 2013), and $\Delta R = 100 \pm 50$.

Core	Core depth (cm)	Lab. ID	Dated bivalve species	^{14}C age (years BP)	Error ($\pm$)	Calibrated age range, $\pm 1\sigma$, $\Delta R = 100 \pm 50$ (years CE/BCE)	Relative probability	Calibrated age, median probability (years CE)
9004	98	Ua-24043	*Nuculana minuta*	710*	35*	1645–1806*	1	1702*
9004	136	Ua-35966	*Nuculana pernula*	675	25	1675–1813	1	1750
9004	164	Ua-23075	*Yoldiella lenticula*	800	40	1538–1664	1	1599
9004	265	Ua-35967	*Nucula* sp.	1025	30	1356–1372/ 1383–1465	0.106/0.894	1416
9004	312	Ua-35968	*Clamys septemradiatus*	1145	25	1295–1389	1	1336
9004	313	Ua-23000	*Abra nitida*	1305*	45*	1138–1276*	1	1195*
9004	371	Ua-35969	*Nucula tenuis*	1245	25	1208–1303	1	1251
9004	492	Ua-23001	*Abra nitida*	1640	45	776–938	1	853
9004	564	Ua-23002	*Nuculana minuta*	1925	40	517–658	1	576
9004	623	Ua-23003	*Thyasira flexuosa*	2155	45	246–410	1	321
9004	705	Ua-23004	*Thyasira flexuosa*	2415	45	68 BCE–102 CE	1	16

* Dates not used in the final age model due to age reversals.

on the correlation of the stable carbon isotopes (δ^{13}C) and benthic foraminiferal species *C. laevigata, Adercotryma glomerata* (Brady, 1878) and *Hyalinea balthica* (Schröter in Gmelin, 1791) with respective data from core G113-091 (Fig. 3b herein; Polovodova Asteman et al., 2013; Polovodova Asteman and Nordberg, 2013). The composite record of GA113-2Aa and 9004 spans from approximately 350 BCE to 1999 CE (Table 2, Fig. 3a), and includes the late Holocene climate events such as the Roman Warm Period (RWP: $\sim$ 350 BCE–450 CE), the Dark Ages Cold Period (DA: $\sim$ 450–850 CE), the Viking Age/Medieval Climate Anomaly (VA/MCA: $\sim$ 850–1350 CE), the Little Ice Age (LIA: $\sim$1350–1850 CE) and the contemporary warming from 1850 CE to present (Lamb, 1995; Filipsson and Nordberg, 2010; Harland et al., 2013, 2017; Polovodova Asteman et al., 2013). We add the Viking Age to the Medieval Climate Anomaly following the approach of Filipsson and Nordberg (2010), based on historical evidence that warming in northern Europe began earlier than 1000 CE, which allowed Vikings to reach the north-east coast of England and loot the monastery of Lindisfarne in 793 CE (Morris, 1985). For further details on the chronology of the GA113-2Aa and 9004 cores see Filipsson and Nordberg (2004a), Polovodova et al., (2011) and Polovodova Asteman et al. (2013).

Combining the long gravity core with the 60 cm long Gemini core, which includes the sediment–bottom water interface and the intact core top, resulted in a high-resolution temporal record of almost 1-year cm^{-1} sample for the upper part of the record and <10 years cm^{-1} sample for the deepest part of the record. Calculations from the ^{210}Pb analyses and the AMS-^{14}C dates suggest sediment accumulation rates of $\sim$ 9 mm year^{-1} in the most recent sediments and approxi-

mately $\sim$ 2.8 mm year^{-1} in the compacted deepest part of the gravity core (Fig. 2). Hence, due to high accumulation rates the upper 60 cm of the record can be directly compared to instrumental hydrographic and meteorological data (Figs. 7 and 8).

4   Stable oxygen isotopes

We measured δ^{18}O on tests of the shallow infaunal foraminifer *Cassidulina laevigata* from the core top samples and from the ca. 8 m long G113-2Aa – 9004 record (Fig. 1b). Between 12 and 20 specimens of *Cassidulina laevigata* were picked from each sample for the analysis. In total 6 and 425 samples were analysed for stable oxygen isotopic composition for the surface sediments and composite G113-2Aa – 9004 record, respectively. All samples were measured at the Department of Geosciences, University of Bremen, Germany, using a Finnigan Mat 251 mass spectrometer equipped with an automatic carbonate preparation device. Isotope composition is given in the usual δ-notation and is calibrated to Vienna Pee Dee Belemnite (V-PDB) standard. The analytical standard deviation is < 0.07 ‰ for δ^{18}O based on the long-term standard deviation of an internal standard (Solnhofen limestone).

The temperature was reconstructed using the salinity–δ^{18}O$_w$ relationship established by Fröhlich et al. (1988) (Eq. 1), which is representative for this region (Filipsson, unpubl. data). An average salinity value of 34.4 (range 33–35) was used in Equation 1, based on instrumental measurements between 1896 and 1999 for the fjord deep water (station Alsbäck Deep). The salinity (S) was assumed to be constant over

the investigated time period.

$$\delta^{18}O_w = 0.272 \times S - 8.91 \tag{1}$$

To calculate temperatures the paleotemperature equation by McCorkle et al. (1997) was applied (Eq. 2). This equation is more appropriate for the temperature range observed in temperate fjord basin than the more commonly used linear equation by Shackleton (1974), which produces unrealistically high temperatures in our study (see results section). The bottom water temperature in degrees Kelvin ($T°K$) was calculated as follows:

$$T°K = \sqrt{\frac{2.78 \cdot 10^3}{\ln(\frac{\delta^{18}O_c + 1000}{0.97006 \cdot \delta^{18}O_w - 29.94} + 1000)} + \frac{2.89}{10^3}}, \tag{2}$$

where $\delta^{18}O_c$ stands for stable oxygen isotopic ratio $^{18}O/^{16}O$ measured in calcite tests of *C. laevigata*, while $\delta^{18}O_w$ is the isotopic composition of water calculated from Equation 1 and converted from SMOW to V-PDB by subtracting 0.27‰ (Bemis et al., 1998).

Finally, to convert reconstructed temperatures to degrees Celsius, Eq. (3) was used:

$$T°C = T°K - 273.15. \tag{3}$$

Since 1990 *C. laevigata* has become a rare species in the Gullmar Fjord deep basin (Fig. 6), which has resulted in a short gap in the most recent part of the record (see discussion). Similar gaps in $\delta^{18}O$ and, hence, in bottom water temperature data are also seen for the earlier part of the record and are due to the absence or very low abundances of *C. laevigata* (Fig. 6).

5 Hydrographical and meteorological instrumental data

Long-term hydrographical instrumental data for temperature, salinity and dissolved oxygen concentration (O_2) for the fjord basin (average for 110–118 m water depth (w.d.)) were extracted from the Swedish Meteorological and Hydrological Institute (SMHI) SHARK database (https://www.smhi.se/klimatdata/oceanografi/havsmiljodata/marina-miljoovervakningsdata; last access: 15 March 2017). Some of the Gullmar instrumental data is also available from the Water Quality Association of the Bohus Coast (BVVF) (http://www.bvvf.se/; last access: 15 March 2017), while the data prior to 1958 was sourced from Engström (1970). The Skagerrak hydrography data for the stations adjacent to OS4-6, 9202, 9205 and OS14 were obtained from the International Council for the Exploration of the Seas (ICES: http://www.ices.dk/marine-data/; last access: 15 March 2017).

Meteorological observations of air temperature were also obtained for Stockholm (https://www.smhi.se/klimatdata; last access: 15 March 2017) and central England (http://www.metoffice.gov.uk/; last access: 16 March 2017), which both have the longest historical meteorological records going as far back as the 18th century.

6 Results

6.1 Core tops

To obtain an error estimate and to facilitate the choice of the paleotemperature equation we used living (stained) tests of *Cassidulina laevigata* from the core top samples collected in the Gullmar Fjord and the adjacent Skagerrak. Calculated bottom water temperatures based on the $\delta^{18}O_c$ values from the living (stained) *C. laevigata* were compared to ICES and SMHI hydrography data from the adjacent stations (Fig. 4a). The $\delta^{18}O_c$ values predicted from the chosen equation (see below) were also used to estimate the reliability of our temperature reconstruction (Fig. 4b). *Cassidulina laevigata* has previously been suggested to calcify 0.19‰ lower than equilibrium (Poole et al., 1994). Our $\delta^{18}O_c$ data from the core tops demonstrate an offset, ranging between 0.01‰ and 0.27‰ (mean 0.15‰), compared with $\delta^{18}O_c$ predicted using the palaeotemperature equation from Mc-Corkle et al. (1997) (Fig. 4b). Applying the mean correction of +0.15‰ to the Gullmar $\delta^{18}O_c$ record results in bottom water temperatures ~0.5–1 °C higher than those recorded by instrumental observations in the fjord (Fig. 2a), while uncorrected $\delta^{18}O_c$ values produce temperatures close to observations. Taking the latter into the account and because, based on available data, it is difficult to estimate how large the correction should be, we further report the uncorrected $\delta^{18}O_c$ values for both the core tops and the sediment cores. Furthermore, we use a median value (0.7 °C) of the range of the produced temperature offset (Fig. 4a) as an error margin for our paleotemperature reconstructions (Figs. 5–6).

Instrumental temperature data from ICES and SMHI were used to calculate $\delta^{18}O_c - \delta^{18}O_w$ for the core top samples to facilitate the choice of a paleotemperature equation. Plotting $\delta^{18}O_c - \delta^{18}O_w$ versus observed temperature data for different paleotemperature equations (Fig. 4c) allowed for an estimation of which of the equations gives the best possible agreement with the core top data; hence, the most appropriate equation could be chosen for temperature reconstructions. Figure 4c shows that $\delta^{18}O$ values from north-western Skagerrak (OS4 and OS6) are clearly in better agreement with equations by Hays and Grossman (1991) and McCorkle et al. (1997), while the central Skagerrak samples (9202 and 9205) plot close to the linear equation by Shackleton (1974). The samples from Gullmar Fjord (G113-091) and the OS14 station, collected just outside the fjord, occupy a space in between the Shackleton equation and those by Hays and Grossman (1991) and McCorkle et al. (1997). This suggests that applying the Shackleton equation for Gullmar Fjord and Skagerrak will result in temperatures higher than observations,
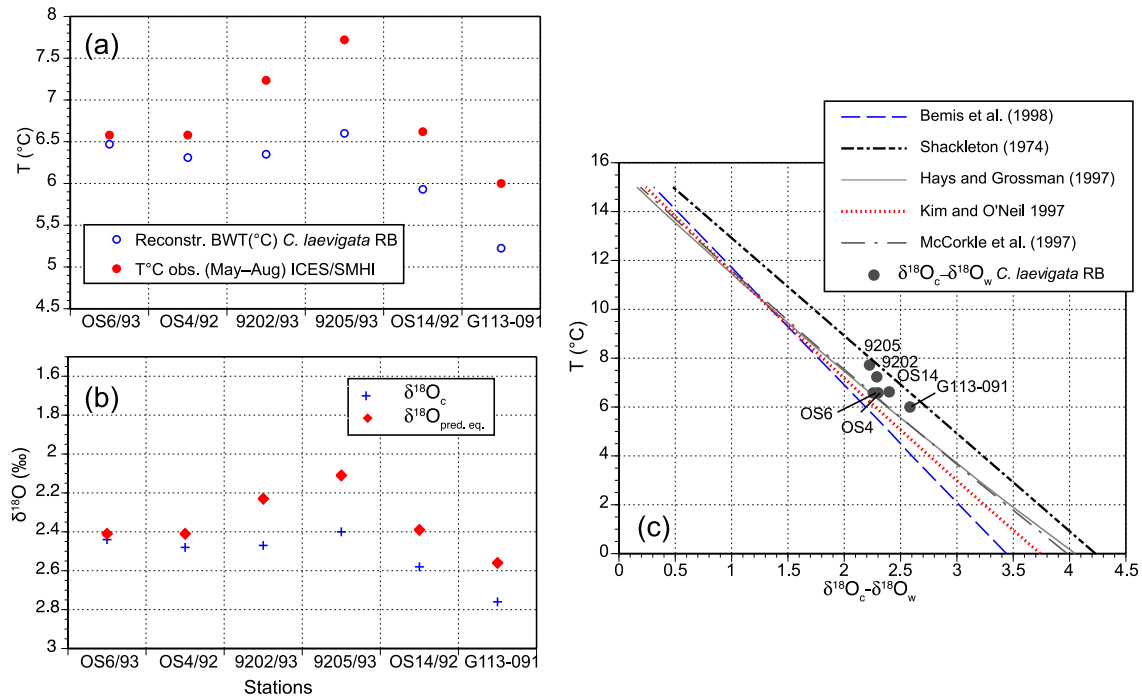
Figure 4. Comparison of reconstructed temperatures and $\delta^{18}O$ values measured in stained *C. laevigata* from the core tops collected in Gullmar Fjord (G113-091) and the Skagerrak (OS4, OS6, OS14, 9202, 9205) to hydrographic temperature data **(a)** and to $\delta^{18}O$ predicted from the palaeotemperature equation **(b)** by McCorkle et al. (1997). **(c)** Temperature vs. $\delta^{18}O_c$–$\delta^{18}O_w$, together with the paleotemperature equations from Shackleton (1974), Hays and Grossman (1991), Kim and O'Neil (1997), McCorkle et al. (1997) and Bemis et al. (1998).

which has been also observed for *Cibicidoides* and *Planulina* from the Florida Straits (Marchitto et al., 2014). Indeed, when testing the Shackleton equation on our dataset, the temperatures are warmer than the ICES hydrographic observation data by 1.5–2 °C. In contrast, the equation by Bemis et al. (1998) applied to the core top $\delta^{18}O_c$ data produces the coldest temperatures, which are 0.9–1.9 °C colder than observations. In turn, it appears that by using Hays and Grossman (1991) or McCorkle et al. (1997) equations, the corresponding calculated temperatures come closer to observations. Both equations are nearly identical for the temperature range from 3 to 8 °C (Fig. 4c) observed between 1890 and 2001 (Fig. 2), and by exercising both equations on the Gullmar Fjord $\delta^{18}O_c$ record almost identical paleotemperature curves are produced. This is rather curious since the equation from Hays and Grossman (1991) is based on meteoric calcite of non-biogenic origin. For this reason, in the current study we apply the McCorkle et al. (1997) equation for the paleotemperature reconstructions.

6.2 Composite record of the G113-2Aa and 9004 sediment cores

The $\delta^{18}O$ record from the Gullmar Fjord shows both decadal and centennial variability for the last 2500 years (Fig. 5a) and can be divided into five major isotopic intervals.

1. For the lower part of the record at 802–592 cm, corresponding to $\sim$ 350 BCE–450 CE, the $\delta^{18}O_c$ values are generally lower ($\sim$ 2.4 ‰) than the long-term average of 2.7 ‰.

2. Between 592 and 475 cm ($\sim$ 450–900 CE) the $\delta^{18}O$ record demonstrates a considerable variability (Fig. 5a), starting with higher $\delta^{18}O_c$ (2.8 ‰–3 ‰) at 592–574 cm ($\sim$ 450–525 CE), which then become lower ($\sim$ 2.4 ‰) at 574–529 cm ($\sim$ 525–700 CE) and increase again ($\sim$ 3.0 ‰) between 529 and 497 cm ($\sim$ 700–825 CE).

3. The 475–302 cm interval ($\sim$ 900–1350 CE) once again displays lower $\delta^{18}O_c$ ($\sim$ 2.4 ‰–2.5 ‰), which are below the long-term average.

4. From 302 to 53.5 cm ($\sim$ 1350–1900 CE) the stable oxygen isotope record increases again with the majority of the $\delta^{18}O_c$ values being $\sim$ 3.1 ‰–3.2 ‰ and exceeding the long-term average. Within this interval the highest $\delta^{18}O$ values of > 3.2 ‰ are found between 300 and 170 cm ($\sim$ 1350 CE–1580 CE).

5. Finally, the $\delta^{18}O$ record becomes lower again ($\sim$ 2.4 ‰) between 53.5 and 5 cm ($\sim$ 1900 and 1996 CE). The $\delta^{18}O$ data for the samples between 5 and 0 cm (1996–1999) are missing because we did not find enough *Cas-*
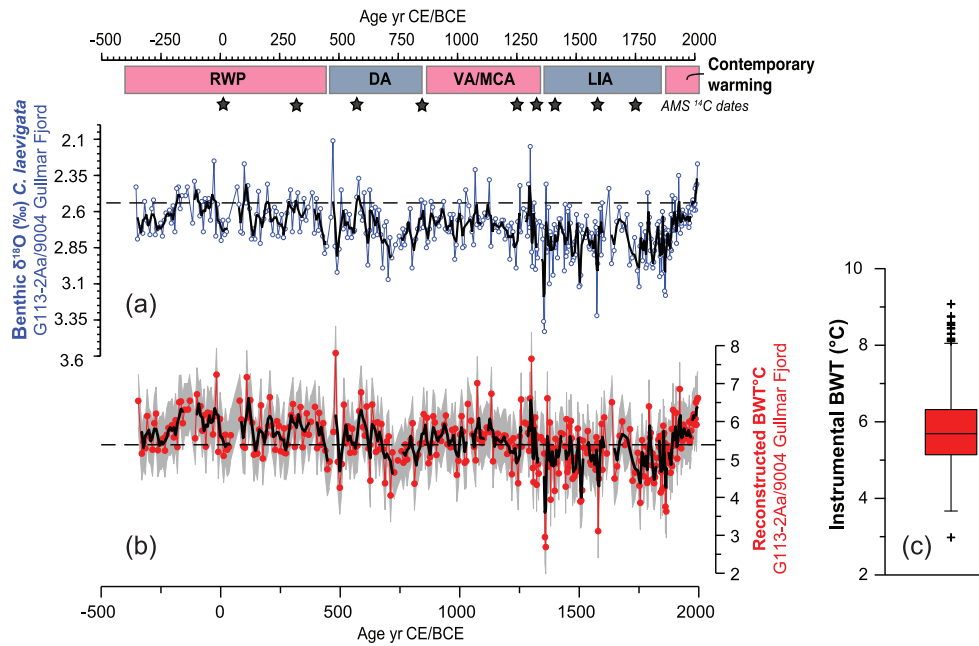
Figure 5. A 2500-year long δ^{18}O record **(a)** and reconstructed winter bottom water temperatures, BWT **(b)** from Gullmar Fjord. Thick lines show the 3-point running mean for both curves, and dashed lines indicate **(a)** a long-term average of 2.4 ‰ for δ^{18}O record and **(b)** 5.4 °C – a mean for instrumental bottom water temperatures registered between 1961 and 1990. Grey shaded areas in BWT indicate a median offset (0.7 °C) in instrumental versus reconstructed temperatures obtained for Rose Bengal stained *C. laevigata* from the core tops (see Fig. 4a), used herein as an error margin. **(c)** The box and whisker plot shows a range for instrumental BWT observations performed from 1890 to 1999 and measured at more regular intervals from the 1960s, the data is from water depths ≥ 110 m in the fjord's deepest basin (Alsbäck Deep). The middle, the upper and the lower horizontal lines in the box indicate the median value and 75th and 25th percentiles, respectively. Abbreviations are as follows: RWP represents the Roman Warm Period, DA represents the Dark Ages, VA/MCA represents the Viking Age/Medieval Climate Anomaly and LIA represents the Little Ice Age.

sidulina laevigata specimens to perform isotopic analyses.

Shifts of ~ 0.25 ‰ in δ^{18}O$_c$ occur throughout the Gullmar Fjord δ^{18}O record, which according to the equation from McCorkle et al. (1997) (used herein) may potentially indicate a temperature variability of ~ 1 °C. The corresponding salinity change is rather small (0.02), and was calculated using the mixing line by Fröhlich et al. (1988) and by applying the δ^{18}O$_c$ range of 2.6–2.85 and a corresponding temperature range of 4.9–5.9 °C. Such salinity changes are well within the amplitude of inter-annual variability (1–1.5), recorded by instrumental salinity observations since the 1890 (Fig. 2b). Foraminifera precipitate their tests during several months (e.g. Filipsson et al., 2004); thus, they integrate the inter-monthly salinity signal, which together with annual variability is minimal according to the instrumental data. For the upper part of the record, the 1 cm sediment slice integrates one or possibly two growing seasons of *C. laevigata* and subsequently records a potentially higher variability of both salinity and temperature. However, in the deepest part of the record a single 1 cm sample may correspond to ~ 7–10 years and is more likely to average inter-annual salinity and temperature variability providing "a more smoothed" signal.

Stable carbon isotope (δ^{13}C) data from the composite G113-2Aa – 9004 record (Filipsson and Nordberg, 2010) were plotted against the oxygen isotope data presented herein, to investigate the potential relationship between the two, e.g., due to different water masses (Supplement Fig. S1). No such relationship was found (Fig. S1), which indicates that our δ^{18}O record mainly reflects fjord deep-water temperatures.

6.3 Reconstructed bottom water temperatures (BWT)

The resulting calculated bottom water temperature record is plotted as both absolute temperature values (Fig. 5b) and as an anomaly from the mean value (5.4 °C), based on the instrumental temperatures observed between 1961 and 1999 (Fig. 6). With very few outliers, the reconstructed temperature range (2.7–7.8 °C) is within the present-day annual variability, documented from instrumental temperature measurements in the fjord's deepest basin since 1890 (Figs. 2a–c, 5c). To further prove that our record represents a winter signal rather than summer conditions (as most biological proxies) we compare the obtained BWT record to instrumental temperatures recorded in the fjord deep water
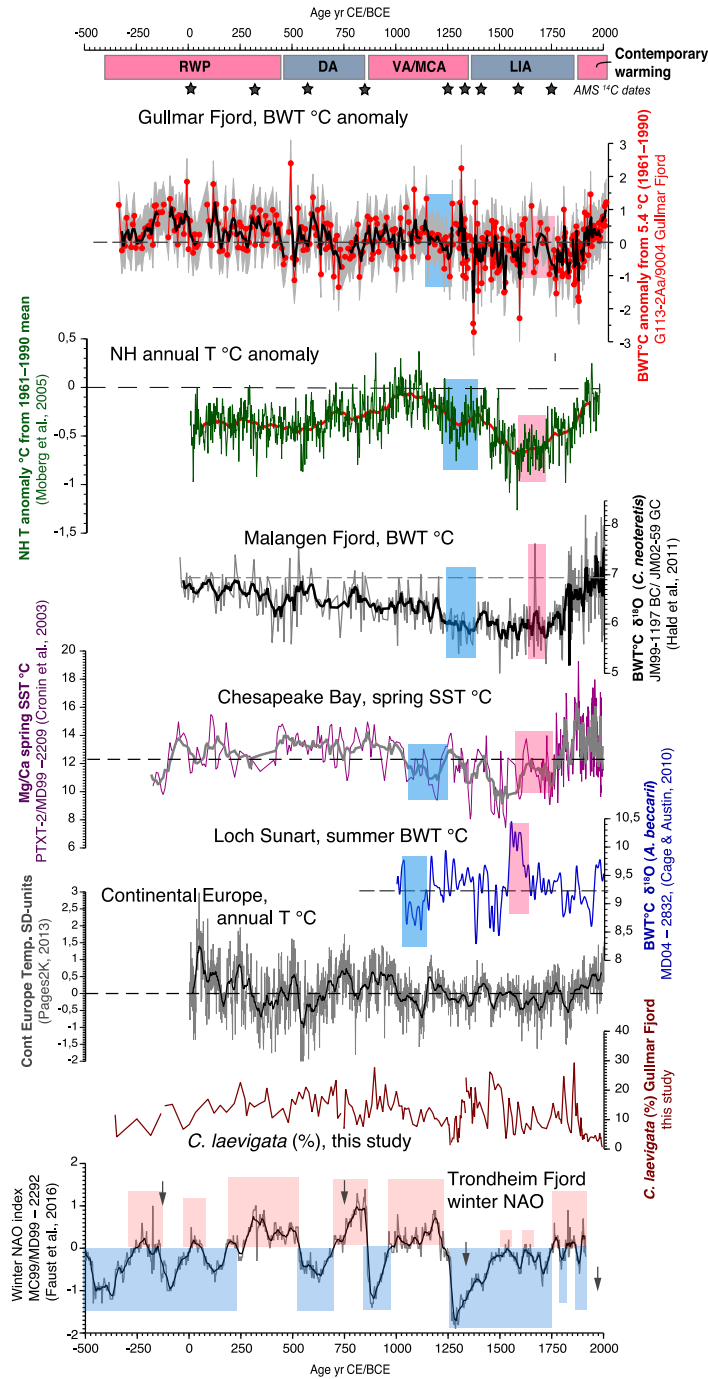
Figure 6. Reconstructed bottom water temperatures (BWT) shown as an anomaly against the 1961–1990 instrumental mean of 5.4 °C from Gullmar Fjord and compared against other temperature proxy records: annual Northern Hemisphere temperatures (Moberg et al., 2005), bottom water temperatures from Malangen Fjord in north-western Norway (Hald et al., 2011) and Loch Sunart in Scotland (Cage and Austin, 2010), spring sea surface temperatures from Chesapeake Bay, eastern North Atlantic Ocean (Cronin et al., 2003), annual temperatures reconstructed for continental Europe (PAGES 2K, 2013) and the reconstructed NAO record from Trondheim Fjord, western Norway (Faust et al., 2016). Also shown, are relative abundances of foraminifer *Cassidulina laevigata* in the fjord with abundance minima and respective gaps in temperature reconstruction linked to the positive NAO index (arrows). For the locations of these proxy records see Fig. 1a and for abbreviations see the caption of Fig. 5. Grey shaded areas in the Gullmar Fjord BWT anomalies indicate a median offset (0.7 °C) in instrumental versus reconstructed temperatures (see Fig. 4a) obtained for Rose Bengal stained *C. laevigata* from the core tops, used herein as an error margin. Blue and pink boxes depict a short-lived cooling at ∼ 1250 CE and a warm interval between ∼ 1570 and 1700 CE, respectively (as discussed in the text).
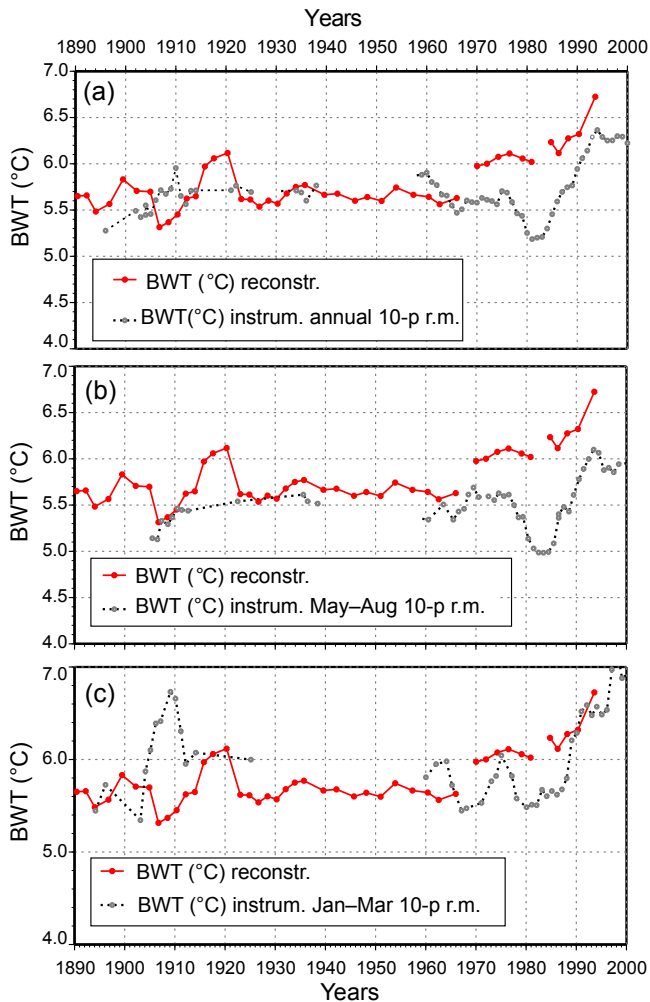
Figure 7. Comparison of the winter bottom water temperatures (BWT) reconstructed from the Gullmar Fjord record to instrumental basin water temperatures measured in the deepest fjord basin: the annual mean **(a)**, the mean for May–August **(b)** and the mean for January–March **(c)**. All instrumental BWT curves (black) are shown as 10-point running means (10-p. r.m.).

during summer and winter. When performing such a comparison, instead of the commonly used June–August (JJA) temperatures for designation of meteorological summer, one has to consider the observations during May–August, when foraminifera precipitate their calcite (Gustafsson and Nordberg, 2001; Filipsson et al., 2004), which is used herein for stable isotope analysis. Likewise, instead of using the months typically employed for the definition of meteorological winter (December–February: DJF), when comparing our record to instrumental data we use January–March. January–March defines "hydrographic winter" in the fjord, and is associated with months when deep-water exchanges occur (see Section 2 of this paper).

Observed annual temperatures registered between 1890 and 1996 (which corresponds to the uppermost part of the

composite G113-2Aa – 9004 record) vary between 3.0 and 8.3 °C, which gives an amplitude of 5.3 °C. Corresponding instrumental 1890–1996 temperatures for the foraminiferal growth season in the fjord (May-August: see above) show a 4.1–7.2 °C range with an amplitude of 5.4 °C. When studying the reconstructed temperatures over the last 2500 years the corresponding amplitude, i.e., the difference between the maximum (7.8 °C) and the minimum (2.7 °C) temperatures is 5.1 °C (Fig. 5b). Furthermore, when plotting the reconstructed bottom water temperatures for the 1890–1996 period versus corresponding instrumental bottom water temperatures as annual averages and means for May–August (Fig. 7b) and January–March (Fig. 7c), the calculated bottom water temperatures and hydrographic data agree with each other rather well in terms of amplitude. However, an increased agreement is reached when comparing the reconstructed data to the hydrographic winter (January–March) temperature (Fig. 7c), which is not surprising considering the fjord hydrography and a season when deep-water exchanges typically occur (see Section 2). Hence, the Gullmar Fjord δ^{18}O-based temperature record reflects the winter temperature variability of surface water in the North Sea.

From the reconstructed Gullmar Fjord temperature record five bottom water temperature intervals can be recognized (Figs. 5b, 6), in parallel to the isotopic intervals mentioned above.

1. From ∼ 350 BCE to 450 CE the fjord bottom water temperatures are consistently above 5.4 °C, the 1961–1990 mean.

2. Between 450 CE and 850 CE the record fluctuates between positive temperature anomalies (∼ 450–650 CE) and negative anomalies (∼ 650–850 CE) reaching minimum value at ∼ 750 CE.

3. At ∼ 850–1300 CE the bottom water temperatures are again above average with a short negative anomaly around 1200–1250 CE.

4. The period between ∼ 1300 CE and 1850 CE in the Gullmar Fjord record is unprecedentedly cold for the last ∼ 2500 years with the majority of temperature anomalies being negative and reaching the minimum value around ∼ 1350 CE (Fig. 6).

5. Finally, from ∼ 1850 CE towards present day the record is characterized by consistently positive bottom water temperature anomalies, which are comparable in the amplitude to the high anomalies found at ∼ 350 BCE–450 CE.

6.4 Gaps in the record due to absent/rare *Cassidulina laevigata*

Some intervals in the G113-2Aa – 9004 record were barren of *C. laevigata* tests; hence, for these intervals, δ^{18}O

values and the corresponding reconstructed bottom water temperature data are missing. These intervals are $\sim$ 130–120 BCE, $\sim$ 725–740 CE, $\sim$ 1260–1265 CE, $\sim$ 1273–1277 CE, $\sim$ 1340 CE and $\sim$ 1996–1999 (Fig. 6). The most recent period of absent/rare *C. laevigata* in the Gullmar Fjord coincides with higher bottom water temperatures and frequently occurring severe hypoxia (see introduction and discussion), as registered by the instrumental measurements in the fjord's deepest basin (Fig. 2c).

7 Discussion

The Gullmar Fjord winter bottom water temperature record shows both centennial and multidecadal variability and has a striking resemblance to climate periods (see below) historically known in northern Europe over the last 2500 years (e.g. Lamb, 1995; Stuiver et al., 1995; Moberg et al., 2005; Filipsson and Nordberg, 2010; Helama et al., 2017). The record demonstrates periods of temperature variability, which correspond to the Roman Warm Period ($\sim$ 350 BCE–450 CE), the Dark Ages cold period ($\sim$ 450–850 CE), the warm Viking Age/Medieval Climate Anomaly ($\sim$ 850–1350 CE), the colder Little Ice Age ($\sim$ 1350–1850 CE) as well as the warmer conditions during the 20th century ($\sim$ 1850 CE–present). There is an overall cooling trend in the Gullmar Fjord temperature record for the last 2500 years, which is consistent with other climate proxy records for this period (e.g. Lebreiro et al., 2006; Eiriksson et al., 2006; Hald et al., 2011; McGregor et al., 2015). Among forcing mechanisms for the late Holocene climate variability in the North Atlantic region changes in temperature and the influx of the Atlantic Water to the region (e.g. Nordberg, 1991; Hass, 1996; Klitgaard-Kristensen et al., 2004; Eiriksson et al., 2006; Lund et al., 2006), radiative forcing (Jiang et al., 2005; Hald et al., 2007), volcanic activity (Otterå et al., 2010; McGregor et al., 2015), land use changes and increased greenhouse gas emissions (e.g. Masson-Delmotte et al., 2013; Abram et al., 2016) are suggested. In addition, there is a strong coupling between atmospheric and ocean circulation, which is linked to the NAO variability. The NAO influences the strength and frequency of moist westerly winds that bring precipitation to northern Europe and has even been suggested to induce multidecadal-scale changes in the AMOC (Dickson et al., 1996), which on centennial scales are linked to the late Holocene major climate extremes (Bianchi and McCave, 1999). Below we discuss each of the climate extremes in detail and compare our record to available temperature proxy data from other settings, highly influenced by the multidecadal NAO variability and climate changes associated with it.

7.1 The Roman Warm Period (prior to $\sim$ 450 CE)

The fjord record shows consistently positive bottom water temperature anomalies during the Roman Warm Period

(RWP) when compared to 5.4 °C, the annual mean for 1961–1999 (Fig. 6). The RWP is often associated with increasingly warm and dry summers both on the British Isles and in central Europe and is linked to the expansion of the Roman Empire (Lamb, 1995; Wang et al., 2012). The RWP warming coincided with a more vigorous flow of the Iceland Scotland Overflow Water, which is an important component of the AMOC (Bianchi and McCave, 1999). Other studies report an increase in the contribution of the Atlantic water to the East Greenland shelf, a reduced sea ice concentration and an increase in the export of fresh water from the Arctic with the East Greenland Current (Fig. 1a), which are all thought to be linked to a shift from the negative to a positive NAO after $\sim$ 500 BCE/0 CE and changes in the AMO regime (e.g. Perner et al., 2015 and references therein; Kolling et al., 2017). Harland et al. (2013) analysed dinoflagellate cysts from the same composite core as presented herein and, based on observed changes in species composition, suggested that sea surface temperatures (SSTs) in the fjord were > 10 °C during the RWP, as compared to present-day SSTs of $\sim$ 9 °C (SMHI, 2017). Other studies suggest SSTs of 6–10 °C for the waters off northern Iceland (Sicre et al., 2011), 10.7–12.6 °C for the Vøring Plateau, Norwegian Sea (Risebrobakken et al., 2011), > 13 °C off north-western Scotland (Wang et al., 2012) and > 15 °C for the Rockall Trough, north-eastern Atlantic (Richter et al., 2009) during this period. Furthermore, for the coastal north-western Atlantic (Chesapeake Bay) SSTs as high as 12–15 °C have been reported (Cronin et al., 2003).

For the adjacent Skagerrak an increase in both intermediate and bottom water temperatures is reported based on Mg / Ca data on benthic foraminiferal species *Melonis barleeanus* (Butruille et al., 2017). Butruille et al. (2017) demonstrate a $\sim$ 2 °C temperature increase and report a temperature range of $\sim$ 6–8 °C during the RWP. In a 2000-year long temperature record from the Malangen Fjord, north-western Norway (Hald et al., 2011), the RWP is characterized as "a warm period with stable bottom water temperatures". The Malangen Fjord record is based on δ^{18}O measured on *Cassidulina neoteretis* Seidenkrantz 1995 and documents a bottom water temperature range of 5.5–7.5 °C (Hald et al., 2011). Both the Skagerrak and Malangen Fjord studies agree well with our dataset, which demonstrates a temperature increase of $\sim$ 2.5 °C, resulting in a 5.4–7.9 °C temperature range during the RWP for the Gullmar Fjord deep water (Fig. 5). The somewhat higher upper range limit of the RWP bottom water temperatures in the Skagerrak and Malangen Fjord, compared to our data, may be explained by the more direct influence of the more temperate Atlantic water at those sites, which may be less prominent in our study area as it is more land-locked and has a stronger continental influence. Also given that our record reflects winter temperatures, its lower BWT temperature range during the RWP is quite reasonable.

When comparing our data to the major temperature synthesis efforts undertaken for the last two millennia, it be-

comes evident that our RWP reconstruction seem to disagree with the Northern Hemisphere temperature record of Moberg et al. (2005), which is mostly characterized by the negative RWP temperature anomalies (Fig. 6). In contrast, the warming seen in the Gullmar Fjord dataset is consistent with the PAGES 2K temperature synthesis for continental Europe (Fig. 6), which also reports a distinct warming corresponding to ∼ 2–3 °C temperature increase during the RWP (PAGES 2K, 2013).

7.2   The Dark Ages Cold Period (∼ 450–850 CE)

Our record displays variable bottom water temperatures in the fjord during the Dark Ages (Figs. 5–6), which is initiated by a short-lived negative anomaly at ∼ 400–450 CE. This anomaly then switches to positive values (∼ 450–650 CE) before once again becoming negative at ∼ 650–850 CE. The Dark Ages Cold Period (DACP) is commonly linked to a large-scale human migration in central Europe (Lamb, 1995; Büntgen et al., 2011). The DACP was contemporaneous with a reduced flow of the Iceland Scotland Overflow Water (Bianchi and McCave, 1999), low solar activity, low pollen influx (Desprat et al., 2003), glacial advance (Lamb, 1995) and a negative mode of the NAO (e.g. Seidenkrantz et al., 2007; Orme et al., 2015; Helama et al., 2017). Summer temperatures < 10 °C in French Alps (Millet et al., 2009), increased humidity in northern Europe (Barber et al., 2004) and a widespread abandonment of arable lands and cultivation in south-western Norway (Salvesen, 1979) were also documented for this period. Furthermore, Seidenkrantz et al. (2007) report a warming of subsurface waters off western Greenland during the DACP attributed to a stronger Atlantic component of the West Greenland Current and a negative NAO.

There is also some cooling during the DACP indicated for the intermediate and deep water in the adjacent Skagerrak (Butruille et al., 2017) but the lower temporal resolution makes it difficult to directly compare the Skagerrak record with ours. In contrast, variable SSTs during the Dark Ages are reported by some North Atlantic records (Sicre et al., 2011; Risebrobakken et al., 2011), with timing similar to the variability of the Gullmar Fjord temperatures (see above). Variable bottom water temperatures are also reported for the Malangen Fjord with a range (5.5–7.5 °C) relatively close to our results (∼ 4–8 °C). There is also some fluctuation between cooling and warming with a ∼ 3–4 °C amplitude in a Mg / Ca-based SST record from Chesapeake Bay (Cronin et al., 2003) and the DACP temperatures reconstructed for continental Europe (PAGES 2K, 2013).

7.3   The Viking Age/Medieval Climate Anomaly (∼ 850–1350 CE)

After the Dark Ages the bottom water temperature anomalies in Gullmar Fjord become positive between ∼ 850 CE and 1350 CE, which fits well with the onset of the warming during the VA/MCA. The warm MCA is believed to be associated with a positive NAO index (e.g. Trouet et al., 2009; Faust et al., 2016), which is likely to have strengthened the AMOC (Bianchi and McCave, 1999) and resulted in an increased transport of heat and moisture to the higher latitudes. The MCA also coincided with grand solar maximum at 1100–1250 CE (Zicheng and Ito, 2000) and its temperature optimum occurred between 1000 CE and 1300 CE, when there was a sharp temperature maximum in most of Europe (Lamb, 1995).

The mean annual northern hemispheric and continental Europe temperature records (Moberg et al., 2005; PAGES 2K, 2013) show the onset of warming as early as between ∼ 850 and 950 CE, with distinct warmth peaks reached around 1000 and 1100 CE and the MCA termination around 1300 CE, which all agrees rather well with our data (Fig. 6). The Malangen Fjord record also already shows warming before 800 CE, which terminates around 1250 CE (Hald et al., 2011), a century earlier than in the Gullmar Fjord record. Despite the inconsistency in timing, which likely results from dating uncertainties (which may be the case for both studies), the two fjord records agree with each other rather well in terms of reconstructed bottom water temperature ranges for this period: 5.4–7.6 °C for the Gullmar Fjord and 5.5–7.1 °C for the Malangen Fjord. In the adjacent Skagerrak both intermediate and deep-water temperatures are reported to increase from ∼ 6 to 8 °C (Butruille et al., 2017) but sampling resolution of the former is too low for the MCA period. In turn, bottom water temperatures in Loch Sunart, in Scotland, increased by ∼ 1.2 °C during the MCA (Cage and Austin, 2010), which is also within the abovementioned ranges. Furthermore, an increase of a similar magnitude during the MCA is reported for the sea surface temperatures in the North Atlantic (Cunningham et al., 2013).

An interesting feature in the Gullmar Fjord record of the VA/MCA is a presence of a short-lived cooling centred at ∼ 1250 CE, before the final peak of warmth at 1250–1350 CE (Fig. 6: see blue box). Such short cooling during the MCA is also documented for both the eastern and western Atlantic coasts (Chesapeake Bay: Cronin et al., 2003; Loch Sunart: Cage and Austin, 2010) but with a slightly different timing, either due to dating uncertainties or the application of different temperature proxies (Mg / Ca vs. δ^{18}O).

7.4   The Little Ice Age (∼ 1350–1850 CE)

From ∼ 1350 to ∼ 1850 CE our record shows winter bottom water temperatures 2–3 °C lower than the instrumental annual mean for 1961–1999 (Fig. 6). Many other proxy records
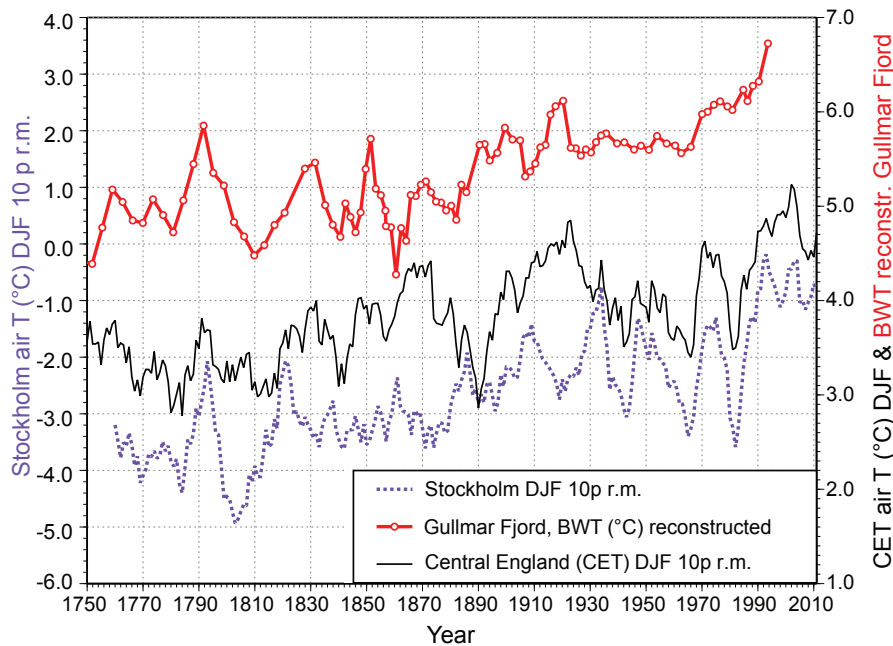
Figure 8. Comparison of reconstructed winter bottom water temperatures (BWT) from Gullmar Fjord to meteorological observations of winter air temperatures recorded for Stockholm (stippled line) and central England (solid line without symbols).

report cooling of a similar magnitude or even stronger in the North Atlantic during the LIA (e.g. Stuiver et al., 1995; Cronin et al., 2003; Klitgaard Kristensen et al., 2004; Eiríksson et al., 2006; Hald et al., 2011; Sicre et al., 2011). The PAGES 2K synthesis of marine palaeoclimate records spanning the past 2000 years also identified a robust global surface ocean cooling with the coldest conditions from 1400 to 1800 CE (McGregor et al., 2015). The Little Ice Age is commonly associated with glacial advances in the Arctic and alpine regions (Porter, 1986; Miller et al., 2012) in response to reduced solar activity (Mauquoy et al., 2002) and summer insolation (Wanner et al., 2011), increased volcanism (Miller et al., 2012), negative North Atlantic Oscillation (e.g. Trouet et al., 2009; Faust et al., 2016) and the reduced strength of the AMOC (e.g. Bianchi and McCave, 1999; Klitgaard Kristensen et al., 2004; Lund et al., 2006). There is also a growing evidence for a stronger Siberian high prevailing from 1450 to 1900 CE based on increased Na^{2+} content in the GISP2 record from Greenland (Mayewski et al., 1997; Meeker and Mayewski, 2002). The onset of the LIA ($\sim$ 1350 CE) on the Swedish west coast also coincided with an outbreak of the Black Death, which decreased the population by 50–60 % and resulted in large-scale farm abandonment with negative implications for land use (Harrison, 2000).

For the Gullmar Fjord a general cooling during the LIA has previously been suggested based on increased abundances of cryophilic dinocysts (Harland et al., 2013) and benthic foraminifer *Adercotryma glomerata*, which prefer bottom water temperatures < 4 °C (Polovodova Asteman et al.,

2013). This agrees rather well with the data presented in this study, which show temperatures as low as $\sim$ 3.4–4.4 °C around 1350, 1500, 1550 and from 1700 to 1850 CE with a general temperature range of 2.9–6.6 °C for the whole LIA period (Fig. 5). Based on foraminiferal faunal and δ^{13}C data Polovodova Asteman et al. (2013) divided the LIA into two distinct phases in the Gullmar Fjord: (1) 1350–1650 CE and (2) 1650–1850 CE, which were separated by a short-lived warming centred at $\sim$ 1650 CE. The reconstructed temperatures also show a short milder episode based on positive anomalies between $\sim$ 1570 and 1700 CE (Fig. 6: see pink box). A similarly warm (but slightly displaced in time) event is visible in other climate records (Fig. 6) from the North Atlantic and Northern Hemisphere (Cronin et al., 2003; Moberg et al., 2005; Cage and Austin, 2010; Hald et al., 2011). This suggests that this short-lived warming was a larger-scale phenomenon possibly linked to a strengthening of the winter NAO, which might have enhanced the AMOC (Cage and Austin, 2010). Indeed, several studies report long-lasting warm conditions in Europe associated with the year 1540 (Casty et al., 2005; Pauling et al., 2006; Wetter et al., 2014), which given our age model uncertainty ($\pm$40 year, see Table 2) for the 1538–1664 CE time interval may well fall within the warm period identified for the LIA from our BWT record. A warming around 1540 is also seen in winter temperature reconstruction for Stockholm ports and harbours based on historical records of sea ice (Leijonhufvud et al., 2009). The model-based reconstruction by Orth et al. (2016) suggests that the European temperatures of 1540 exceeded

those of the 2003 summer, which was likely the warmest for centuries (e.g. Luterbacher et al, 2016). However, this is difficult to deduce based on the data presented herein, as (i) the fjord BWT represent winter temperatures and (ii) the record only stretches until ∼ 1996.

The climax or the coldest part of the LIA is often linked to the Maunder minimum in solar activity, which occurred at ∼ 1645–1715 CE (Mauquoy et al., 2002). Our record shows a distinct cooling at around 1750 CE with temperatures ∼ 1 °C below the 1961–1999 mean, which given a calibrated ^{14}C age range for this particular date (1675–1813 CE ±25 years; see Table 2), may well represent the Maunder minimum in our record. At the same time, a 500-year long reconstruction of Stockholm winter temperatures based on sea ice records from local ports and harbours does not show the coldest temperatures during the LIA climax, instead demonstrating that the coldest decade for the last 500 years occurred from 1592 to 1601 CE with average negative temperature anomalies of ∼ −4 °C (Leijonhufvud et al., 2009).

It is rather intriguing that the coldest bottom water temperatures for the last 2500 years in the Gullmar Fjord are associated with the onset of the LIA (1350 CE, ∼ 2 °C colder than the 1961–1999 mean) rather than with its climax (Figs. 5–6). This agrees well with the LIA temperature evolution reported for Loch Sunart (Cage and Austin, 2010) and Chesapeake Bay (Cronin et al., 2003), which both show 2–4 °C cooling of the bottom waters at the MCA–LIA transition (Fig. 6), attributed to a switch from the positive winter NAO mode dominating during the medieval times (e.g. Trouet et al., 2009; Faust et al., 2016) to the negative NAO prevailing during the major part of the Little Ice Age. Such a switch in the NAO has been linked to a relaxation of the persistent La-Niña-like conditions in the equatorial Pacific dominating the MCA (Trouet et al., 2009). The MCA–LIA transition has been dated to 1250 CE (Cunningham et al., 2013), 1400 CE (McGregor et al., 2015) and 1450 CE (Cage and Austin, 2010), in contrast to our study (1350 CE), which may again be a result of ^{14}C dating uncertainties valid for all of the above-mentioned marine records. At the same time the Chesapeake Bay study places the MCA–LIA transition between 1300 and 1400 CE (Cronin et al., 2003), which agrees with our data.

Another interesting feature of the LIA climate variability is associated with consistently low fjord BWT as well as reduced air temperatures during the 1790–1820 CE period as indicated by the Stockholm and central England instrumental time series (Fig. 8). Despite that this time period is known to coincide with the Dalton minimum in solar activity (Grove, 1988) it is suggested that volcanic activity played a much more important role in climate cooling (e.g. Wagner and Zorita, 2005; McGregor et al., 2015). The role of AMOC strength in shaping the LIA cold periods is also somewhat controversial based on marine geological evidence: whilst the AMOC weakening was proposed as a trigger for the LIA cooling (Bianchi and McCave, 1999), it was argued against (Keigwin and Boyle, 2000) and was not

statistically significant in paleoclimate modelling (Van der Schrier and Barkmeijer, 2005). It has even been suggested that the Gulf Stream may have experienced warming during this period (e.g. Keigwin and Pickart, 1999), which certainly does not explain low BWT temperatures in our record or low air temperatures over Stockholm and central England during 1790–1820 CE. An explanation for this phenomenon has been proposed by Bjerknes (1965), who postulated that "a decrease in the western European winter surface air temperatures from 1790 to 1820 CE was almost completely related to the anomalous southward advection of cold polar air", a hypothesis later supported by a model study by Van der Schrier and Barkmeijer (2005).

7.5 The Contemporary Warm Period (∼ 1850 CE–1996)

Most of the proxy records in the North Atlantic indicate a clear warming trend for the last 100–200 years (Hald et al., 2011, and references therein) and so do our data, which pick up the warm 1930s and the 1990s (Fig. 8). The 500-year long reconstruction of Stockholm winter temperatures also demonstrates that the 20th century has experienced four out of the five warmest decades over the last 500 years: 1905–1914, 1930–1939, 1989–1998 and 1999–2008 (Leijonhufvud et al., 2009). The Gullmar Fjord temperature record shows that when considering a 3-point running mean temperature variability, the most recent warming does not stand out in comparison to the RWP and the MCA, as has also been previously demonstrated by other studies such as a tree ring-based summer temperature record from central Scandinavia (Linderholm and Gunnarson, 2005), Scottish loch data (Cage and Austin, 2010), North Atlantic SST composite data (Cunningham et al., 2013) and a 2000-year temperature record for continental Europe (PAGES 2K, 2013). At the same time, this "not outstanding recent warming" seen in our dataset is in contrast to the Malangen Fjord record (Hald et al., 2011), which infers that the last 100 years have been the warmest in the last two millennia. This may reflect the so-called polar amplification, as suggested by Hald et al. (2011), since Malangen Fjord is located much further to the north than Loch Sunart and Gullmar Fjord, which are both comparably temperate fjord inlets. On the other hand, the stronger recent warming of the Norwegian fjord record may also be explained by a more direct link to the northward flow of the Atlantic water as compared to Gullmar Fjord, which is (i) not located within the core of the North Atlantic Current (Fig. 1) and (ii) reflects temperature variability during the winter season. At the same time, the spring SST reconstruction from Chesapeake Bay (Cronin et al., 2003; Fig. 6 herein) shows that the 20th century warming clearly exceeds temperatures observed during the prior 2500 years. The shallow Chesapeake Bay displays large seasonal temperature and salinity variability (Cronin et al., 2003) in contrast to Gullmar Fjord, Malangen Fjord and Loch Sunart, which all have slightly/less variable bottom water conditions during the year and

similar "fjordic" circulation with annual or less frequent basin water exchanges. Furthermore, the SST record from the Chesapeake Bay is the shallowest temperature reconstruction (12–25 m w.d.) among the temperature records considered in this study (Loch Sunart: 56 m; Gullmar Fjord: 120 m; and Malangen Fjord: 218 m w.d.). Shallow water areas are known to generally warm up faster, especially given the facilitating atmospheric warming of the late 20th century due to the increase in greenhouse gas emissions (e.g. Masson-Delmotte, 2013); this may also explain why the recent SST increase in the Chesapeake Bay record is unprecedented in a 2500-year perspective.

Studying the instrumental hydrographic time series from the Gullmar Fjord plotted versus reconstructed temperatures (Fig. 7), it is clear that our record captures the most recent warm period with the bottom water temperatures that have increased by $\sim 1.5\,°C$ since the 1960s. A similar increase has been documented for Loch Sunart (Cage and Austin, 2010) and Ranafjorden, on the north-west coast of Norway (Klitgaard-Kristensen et al., 2004). Instrumental meteorological time series for air temperatures since 1960s from Stockholm and central England also demonstrate a winter temperature increase of 3–3.5 °C, which is higher than the reconstructed range of Gullmar Fjord bottom water temperatures for this period (Fig. 8). Overall, the variability in the reconstructed fjord temperatures corresponds well with both meteorological datasets from 1750 to 1990, with the exception of an individual wiggle mismatch between 1930 and 1990 (Fig. 8). In general, it appears that both air temperatures records lead the observed variability while bottom water temperatures are lagging behind for the 1930–1990 period (Fig. 8).

Our record also shows higher BWT prior to the 1920s (Fig. 8), which coincides with the cold AMO (low SSTs) and low sea surface salinities in the North Atlantic and subpolar gyre (Reverdin et al. 1994; Reverdin, 2010); however, in the following period until ~ 1960, the reconstructed BWT remains at a lower level (during the warm AMO, i.e., high North Atlantic SSTs), after which it peaks again during the "Great Salinity Anomaly" in the late 1970s and late 1980s (Dickson et al., 1988; Belkin et al., 1998). Nevertheless, it remains intriguing that on both occasions (prior to the 1920s and during the 1970s/1980s) of reduced salinities and low SSTs in the North Atlantic, our record is characterized by high fjord deep water temperatures, which is consistent with increasing air temperatures in instrumental datasets from Stockholm and central England (Fig. 8). The low surface salinities of the Great Salinity Anomaly were likely driven by an increased freshwater/sea ice export from the Arctic via Fram Strait and the Canadian Archipelago (Belkin et al., 1998). The increased freshwater flux into the subpolar North Atlantic is, in turn, suggested to have increased the salinity of the North Atlantic Current, which may have reduced its predicted weakening due to enhanced freshwater fluxes and would have helped

to restart a stronger AMOC (Hátún et al., 2005; Thornalley et al., 2009). A stronger North Atlantic Current would subsequently have resulted in an increased heat transport during winter to the eastern North Atlantic and in combination with other external forcing factors (e.g. changes in NAO, volcanism, and solar activity) would have contributed to the warming observed in the fjord BWT record during the early 20th century. One of those factors, the positive NAO mode, which has prevailed since the 1970s/1980s (Hurrell, 1995; http://www.cpc.ncep.noaa.gov/products/precip/CWlink/pna/season.JFM.nao.gif; last access: 15 March 2017), extracts heat from the subpolar North Atlantic through increased westerlies over that region, decreases SSTs, enhances convection, increases ocean density (Delworth et al., 2016; Delworth and Zeng, 2016) and results in milder winter conditions over north-western Europe; thus, it counteracts the effects of the AMOC weakening, which has been suggested for the 20th century based on modelling data and proxy records (Caesar et al., 2018; Thornalley et al., 2018). Furthermore, as it is located within a coastal region, the Gullmar Fjord is more susceptible to wind-forced temperature changes, which follow the variability of the NAO index and drive coastal upwelling and downwelling in the fjord (Björk and Nordberg, 2003). According to Jansen et al. (2007), the late 20th century warming, as demonstrated by many proxy records from the north-eastern Atlantic (see discussion above), is unlikely to be explained by external forcing factors and is probably linked to anthropogenic drivers such as greenhouse gas emissions and aerosols (Booth et al., 2012), which have both significantly increased since ~ 1970s (Masson-Delmotte, 2013).

When studying the Gullmar Fjord bottom water temperature record for the last 2500 years, it is interesting to note that the most recent warming of the 20th century (presented herein until 1996) does not stand out, and it actually appears to be comparable to both the Roman Warm Period and the Medieval Climate Anomaly. However, this observation must be interpreted with caution, as our dataset does not go beyond year 1996 due to a lack of material (see discussion below); hence, it does not cover the most recent part of the 20th century warming, which is widely accepted as having been triggered by growing anthropogenic emissions.

7.6 Environmental conditions explaining the absence or rare occurrence of *Cassidulina laevigata* in the record

Since 1990, *Cassidulina laevigata* has dramatically decreased in abundance in the Gullmar Fjord deep basin (Fig. 6). A similar pattern, with short disappearances of *C. laevigata*, is seen during the Roman and Medieval warm periods (Fig. 6). This effect may either be due to increased temperatures and/or, more likely, due to periods of severe hypoxia as *C. laevigata* is documented to be sensitive to oxygen concentrations below $1\,mL\,L^{-1}$ (e.g. Gustafsson and Nord-

berg, 2001; Nardelli et al., 2014). To a large extent, the oxygen status of fjords and estuaries on the Swedish west coast, is controlled by climate (e.g. Nordberg et al., 2000; Filipsson and Nordberg 2004a, b), but the late Holocene changes in land use and organic enrichment in the fjord are also suggested to have played a role (Filipsson and Nordberg, 2010). Thus, the short extinctions of *C. laevigata* during warmer periods in the past may be equivalent to the present-day pattern of severe hypoxia following the positive NAO periods with mild and humid winters, limited basin water exchange and high organic matter flux increasing oxygen demand (Nordberg et al., 2000, 2001; Filipsson and Nordberg 2004a). Indeed, when comparing our record to the reconstructed NAO index from the Trondheim Fjord in western Norway (Faust et al., 2016) it appears that sediment core intervals with absent *C. laevigata* (at ∼ 75, 450, 1000 CE and post-1990) correlate rather well with the positive NAO index (Fig. 6).

8 Conclusions

To conclude, from the available paleotemperature equations, the equation by McCorkle et al. (1997) produced the most realistic reconstructed deep water temperature range of 2.7–7.8 °C, which falls within the annual variability instrumentally recorded in the deep fjord basin since 1890. This suggests that the Gullmar Fjord δ^{18}O record mainly reflects the variability of the winter bottom water temperatures with a minor salinity influence. The relationship between the evolution of the fjord's bottom water temperatures over the last two millennia and other late Holocene climate records reveals synchronous North Atlantic-wide centennial and multidecadal climate variability despite age model uncertainties, different proxy type, time resolution, annual versus seasonal signal and different hydrographic characteristics.

The record shows a substantial and long-term warming during the Roman Warm Period (∼ 350 BCE–450 CE), followed by variable bottom water temperatures during the Dark Ages (∼ 450–850 CE). The Viking Age/Medieval Climate Anomaly (∼ 850–1350 CE) is also indicated by positive bottom water temperature anomalies, while the Little Ice Age (∼ 1350–1850 CE) is characterized by a long-term cooling with distinct multidecadal variability. The record also picks up the contemporary warming of the 1930s and the 1990s. When studying the Gullmar Fjord bottom water temperature record for the last 2500 years, it is interesting to note that the warming of the 20th century (presented herein until 1996) is comparable to both the Roman Warm Period and the Medieval Climate Anomaly.

Information about the Supplement

Figure S1 contains a scatter plot of stable carbon isotope (δ^{13}C) data from the composite G113-2Aa – 9004 record (Filipsson and Nordberg, 2010) plotted against the oxygen isotope data presented herein. Note absence of a correlation between the two, ruling out the possibility that the changes in δ^{18}O are due to changes in water masses.

References

Abram, N. J., McGregor, H. V., Tierney, J. E., Evans, M. N., McKay, N. P., Kaufman, D. S., and PAGES 2k Consortium: Early onset of industrial-era warming across the oceans and continents, Nature, 536, 411–418, 2016.

Appleby, P. G. and Oldfield, F.: The calculation of lead-210 dates assuming a constant rate of supply of unsupported ^{210}Pb to the sediment, Catena, 5, 1–8, 1978.

Arneborg, L.: Turnover times for the water above sill level in Gullmar Fjord, Cont. Shelf Res., 24, 443–460, 2004.

Årthun, M., Eldevik, T., Viste, E., Drange, H., Furevik, T., Johnson, H. L., and Keenlyside, N. S.: Skillful prediction of northern climate provided by the ocean, Nat. Commun., 8, 15875, https://doi.org/10.1038/ncomms15875, 2017.

Barber, K. E., Chambers, F. M., and Maddy, D.: Late Holocene climatic history of northern Germany and Denmark: peat macrofossil investigations at Dosenmoor, Schleswig– Holstein and, Svanemose, Jutland, Boreas, 33, 132–144, 2004.

Belkin, I. M., Levitus, S., Antonov, J., and Malmberg, S. A.: "Great salinity anomalies" in the North Atlantic, Prog. Oceanogr., 41, 1–68, 1998.

Bemis, B. E., Spero, H. J., Bijma, J., and Lea, D. W.: Reevaluation of the oxygen isotopic composition of planktonic foraminifera: Experimental results and revised paleotemperature equations, Paleoceanography, 13, 150–160, 1998.

Bianchi, G. G. and McCave, I. N.: Holocene periodicity in North Atlantic climate and deep-ocean flow south of Iceland, Nature, 397, 515–517, 1999.

Bjerknes, J.: Atmosphere-ocean interaction during the "Little Ice Age", in: WMO-IUGG Symposium on Research and Development Aspects of Longe-Range Forecasting WMO-No. 162. TP. 79, Technical Note No. 66, 77–88, 1965.

Björk, J. and Nordberg, K.: Upwelling along the Swedish west coast during the 20th century, Cont. Shelf Res., 23, 1143–1159, 2003.

Booth, B. B., Dunstone, N. J., Halloran, P. R., Andrews, T., and Bellouin, N.: Aerosols implicated as a prime driver of twentieth-century North Atlantic climate variability, Nature, 484, 228–234, 2012.

Bronk Ramsey, C.: Improving the resolution of radiocarbon dating by statistical analysis, in: Radiocarbon Dating: Archaeology, Text and Science, edited by: Levy, T. E. and Higham, T. F. G., The Bible and Equinox, London, 57–64, 2005.

Büntgen, U., Tegel, W., Nicolussi, K., McCormick, M., Frank, D., Trouet, V., Kaplan, J. O., Herzig, F., Heussner, K. U., Wanner, H., Luterbacher, J., and Esper, J.: 2500 Years of European Climate Variability and Human Susceptibility, Science, 331, 578–582, 2011.

Butler, P. G., Wanamaker, A. D., Scourse, J. D., Richardson, C. A., and Reynolds, D. J.: Variability of marine climate on the North Icelandic Shelf in a 1357-year proxy archive based on growth increments in the bivalve Arctica islandica, Palaeogeogr. Palaeocl., 373, 141–151, 2013.

Butruille, C., Krossa, V. R., Schwab, C., and Weinelt, M.: Reconstruction of mid-to late-Holocene winter temperatures in the Skagerrak region using benthic foraminiferal Mg / Ca and δ^{18}O, The Holocene, 27, 63–72, 2017.

Caesar, L., Rahmstorf, S., Robinson, A., Feulner, G., and Saba, V.: Observed fingerprint of a weakening Atlantic Ocean overturning circulation, Nature, 556, 191–198, 2018.

Cage, A. G. and Austin, W. E. N.: Marine climate variability during the last millennium: the Loch Sunart record, Scotland, UK, Quaternary Sci. Rev., 29, 1633–1647, 2010.

Casty, C., Wanner, H., Luterbacher, J., Esper, J., and Böhm, R.: Temperature and precipitation variability in the European Alps since 1500, Int. J. Climatol., 25, 1855–1880, 2005.

Central England air temperature dataset: http://www.metoffice.gov.uk/, last access: 16 March 2017.

Cronin, T. M., Dwyer, G. S., Kamiya, T., Schwede, S., and Willard, D. A.: Medieval Warm Period, Little Ice Age and 20th century variability from Chesapeake Bay, Glob. Planet. Change, 36, 17–29, 2003.

Cunningham, L. K., Austin, W. E., Knudsen, K. L., Eiríksson, J., Scourse, J. D., Wanamaker Jr., A. D., Butler, P. G., Cage, A. G., Richter, T., Husum, K., Hald, M., Andersson, C., Zorita, E., Linderholm, H. W., Gunnarsson, B., Sicre, M.-A., Sejrup, H. P., Jiang, H., and Wilson, R. J. S.: Reconstructions of surface ocean conditions from the northeast Atlantic and Nordic seas during the last millennium, The Holocene, 23, 921–935, 2013.

Curry, R. G. and McCartney, M. S.: Ocean gyre circulation changes associated with the North Atlantic Oscillation, J. Phys. Oceanogr., 31, 3371–3400, 2001.

Delworth, T. L. and Zeng, F.: The impact of the North Atlantic Oscillation on climate through its influence on the Atlantic Meridional Overturning Circulation, J. Clim., 29, 941–962, 2016.

Delworth, T. L., Zeng, F., Vecchi, G. A., Yang, X., Zhang, L., and Zhang, R.: The North Atlantic Oscillation as a driver of rapid climate change in the Northern Hemisphere, Nat. Geosci., 9, 509–513, 2016.

Desprat, S., Goñi, M. F. S., and Loutre, M. F.: Revealing climatic variability of the last three millennia in northwestern Iberia using pollen influx data, Earth Planet. Sc. Lett., 213, 63–78, 2003.

Dickson, R., Lazier, J., Meincke, J., Rhines, P., and Swift, J.: Long-term coordinated changes in the convective activity of the North Atlantic, Prog. Oceanogr., 38, 241–295, 1996.

Dickson, R. R., Meincke, J., Malmberg, S.-A., and Lee, A. J.: The "Great Salinity Anomaly" in the northern North Atlantic, 1968–1982, Prog. Oceanogr., 20, 103–151, 1988.

Eiríksson, J., Bartels-Jonsdottir, H. B., Cage, A. G., Gudmundsdottir, E. R., Klitgaard-Kristensen, D., Marret, F., Rodrigues, T., Abrantes, F., Austin, W. E. N., Jiang, H., Knudsen, K. L., and Sejrup, H. P.: Variability of the North Atlantic Current during the last 2000 years based on shelf bottom water and sea surface temperatures along an open ocean/shallow marine transect in western Europe, The Holocene, 16, 1017–1029, 2006.

Enfield, D. B., Mestas-Nuñez, A. M., and Trimble, P. J.: The Atlantic multidecadal oscillation and its relation to rainfall and river flows in the continental US, Geophys. Res. Lett., 28, 2077–2080, 2001.

Faust, J. C., Fabian, K., Milzer, G., Giraudeau, J., and Knies, J.: Norwegian fjord sediments reveal NAO related winter temperature and precipitation changes of the past 2800 years, Earth Planet. Sc. Lett., 435, 84–93, 2016.

Filipsson, H. L. and Nordberg, K.: Climate variations, an overlooked factor influencing the recent marine environment. An example from Gullmar Fjord, Sweden, illustrated by benthic

foraminifera and hydrographic data, Estuaries, 27, 867–881, 2004a.

Filipsson, H. L. and Nordberg, K.: A 200-year environmental record of a low-oxygen fjord, Sweden, elucidated by benthic foraminifera, sediment characteristics and hydrographic data, J. Foramin. Res., 34, 277–293, 2004b.

Filipsson, H. L. and Nordberg, K: Variations in organic carbon flux and stagnation periods during the last 2400 years in a Skagerrak fjord basin, inferred from benthic foraminiferal δ^{13}C, in: Fjords: Depositional Systems and Archives, Geological Society Special Publication, edited by: Howe, J. A., Austin, W. E. N., Forwick, M., Powell, R. D., and Paetzel, M., 261–270, 2010.

Filipsson, H. L., Nordberg, K., and Gustafsson, M.: Seasonal study of δ^{18}O and δ^{13}C in living (stained) benthic foraminifera from two Swedish fjords, Mar. Micropal., 53, 159–172, 2004.

Filipsson, H. L., Bernhard, J. M., Lincoln, S. A., and McCorkle, D. C.: A culture-based calibration of benthic foraminiferal paleotemperature proxies: δ^{18}O and Mg / Ca results, Biogeosciences, 7, 1335–1347, https://doi.org/10.5194/bg-7-1335-2010, 2010.

Fröhlich, K., Grabczak, J., and Rozanski, K.: Deuterium and oxygen-18 in the Baltic Sea, Chem. Geol., 72, 77–83, 1988.

Grove, J.: The Little Ice Age, Methuen and Co, London, 498 pp., 1988.

Gunnarson, B. E., Linderholm, H. W., and Moberg, A.: Improving a tree-ring reconstruction from west-central Scandinavia: 900 years of warm-season temperatures, Clim. Dynam., 36, 97–108, 2011.

Gustafsson, M. and Nordberg, K.: Living (stained) benthic foraminiferal response to primary production and hydrography in the deepest part of the Gullmar Fjord, Swedish West Coast, with comparisons to Hoglund's 1927 material, J. Foramin. Res., 31, 2–11, 2001.

Hald, M., Andersson, C., Ebbesen, H., Jansen, E., Klitgaard-Kristensen, D., Risebrobakken, B., Salomonsen, G. R., Sarnthein, M., Sejrup, H. P., and Telford, R. J.: Variations in temperature and extent of Atlantic Water in the northern North Atlantic during the Holocene, Quaternary Sci. Rev., 26, 3423–3440, 2007.

Hald, M., Salomonsen, G. R., Husum, K., and Wilson, L. J.: A 2000-year record of Atlantic Water temperature variability from the Malangen Fjord, northeastern North Atlantic, The Holocene, 21, 1049–1059, 2011.

Hansen, B. and Østerhus, S.: North Atlantic-Nordic seas exchanges, Prog. Oceanogr., 45, 109–208, 2000.

Harland, R., Nordberg, K., and Filipsson, H. L.: Dinoflagellate cysts and hydrographical change in Gullmar Fjord, west coast of Sweden, Sci. Total Environ., 355, 204–231, 2006.

Harland, R., Polovodova Asteman, I., and Nordberg, K.: A two-millennium dinoflagellate cyst record from Gullmar Fjord, a Swedish Skagerrak sill fjord, Palaeogeogr. Palaeocl., 392, 247–260, 2013.

Harrison, D.: Stora Döden/ The Black Death, Stockholm, Ordfront, 2000 (in Swedish).

Hass, H. C.: Northern Europe climate variations during late Holocene: evidence from marine Skagerrak, Palaeogeogr. Palaeocl., 123, 121–145, 1996.

Hátún, H., Sandø, A. B., Drange, H., Hansen, B., and Valdimarsson, H.: Influence of the Atlantic subpolar gyre on the thermohaline circulation, Science, 309, 1841–1844, 2005.

Hays, P. D. and Grossman, E. L.: Oxygen isotopes in meteoric calcite cements as indicators of continental paleoclimate, Geology, 19, 441–444, 1991.

Helama, S., Jones, P. D., and Briffa, K. R.: Dark Ages Cold Period: a literature review and directions for future research, The Holocene, 27, 1600–1606, 2017.

Howe, J. A., Austin, W. E. N., Forwick, W., Paetzel, M., Harland, R., and Cage, A. G.: Fjord systems and archives: a review, in: Fjords: Depositional Systems and Archives, edited by: Howe, J. A., Austin, W. E. N., Forwick, M., and Paetzel, M., Geol. Soc. Spec. Publ., 344, 261–270, 2010.

Hurrell, J. W.: Decadal trends in the north-Atlantic oscillation – regional temperatures and precipitation, Science, 269, 676–679, 1995.

ICES database: http://www.ices.dk/marine-data/, last access: 8 March 2017.

Jackson, L. C., Kahana, R., Graham, T., Woollings, T., Mecking, J. V., and Wood, R. A.: Global and European climate impacts of a slowdown of the AMOC in a high resolution GCM, Clim. Dynam., 45, 3299–3316, 2015.

Jansen, E., Overpeck, J., Briffa, K. R., Duplessy, J. C., Joos, F., Masson-Delmotte, V., Olago, D., Otto-Bliesner, B., Peltier, W. R., Rahmstorf, S., Ramesh, R., Raynaud, D., Rind, D., Solomina, O., Villalba, R., and Zhang, D.: Paleoclimate, in: IPCC WG1 Fourth Assessment Report, edited by: Solomon, S., Qin, D., Manning, M., Chen, Z., Marquis, M., Averyt, K. B., Tignor, M., and Miller, H. L., Climate Change 2007, The Physical Science Basis, Cambridge Univ. Press, 433–498, 2007.

Jiang, H., Eiríksson, J., Schulz, M., Knudsen, K. L., and Seidenkrantz, M. S.: Evidence for solar forcing of sea-surface temperature on the North Icelandic Shelf during the late Holocene, Geology, 33, 73–76, 2005.

Keigwin, L. D. and Boyle, E. A.: Detecting Holocene changes in thermohaline circulation, P. Natl. Acad. Sci. USA, 97, 1343–1346, 2000.

Keigwin, L. D. and Pickart, R. S.: Slope Water Current over the Laurentide Fan on Interannual to Millenial Time Scales, Science, 286, 520–523, 1999.

Kim, S. T. and O'Neil, J. R.: Equilibrium and nonequilibrium oxygen isotope effects in synthetic carbonates, Geochim. Cosmochim. Ac., 61, 3461–3475, 1997.

Kjennbakken, H., Sejrup, H. P., and Haflidason, H.: Mid-to late-Holocene oxygen isotopes from Voldafjorden, western Norway, The Holocene, 21, 897–909, 2011.

Klitgaard-Kristensen, D., Sejrup, H. P., Haflidason, H., Berstad, I. M., and Mikalsen, G.: Eight-hundred-year temperature variability from the Norwegian continental margin and the North Atlantic thermohaline circulation, Paleoceanography, 19, PA2007, https://doi.org/10.1029/2003PA000960, 2004.

Knox, J., Daccache, A., Hess, T., and Haro, D.: Meta-analysis of climate impacts and uncertainty on crop yields in Europe, Env. Res. Lett., 11, 113004, 2016.

Kolling, H., Stein, R., Fahl, K., Perner, K., and Moros, M.: Short-term variability in late Holocene sea ice cover on the East Greenland shelf and its driving mechanisms, Palaeogeogr. Palaeocl., 485, 336–350, 2017.

Kuhlbrodt, T., Rahmstorf, S., Zickfeld, K., Vikebø, F., Sundby, S., Hofmann, M., Link, P., Bondeau, A., Cramer, W., and Jaeger, C.:

An integrated assessment of changes in the thermohaline circulation, Climatic Change, 96, 489–537, 2009.

Lamb, H. H.: 1977 Climate: present, past and future, New York, Methuen, 1995.

Lebreiro, S. M., Francés, G., Abrantes, F. F. G., Diz, P., Bartels-Jónsdóttir, H. B., Stroynowski, Z. N., Gil, I.M., Pena, L. D., Rodrigues, T., Jones, P. D., Nombella, M. A., Alejo, I., Briffa, K. R., Harris, I., and Grimalt, J. O.: Climate change and coastal hydrographic response along the Atlantic Iberian margin (Tagus Prodelta and Muros Ría) during the last two millennia, The Holocene, 16, 1003–1015, 2006.

Leijonhufvud, L., Wilson, R., Moberg, A., Soderberg, J., Retso, D., and Soderlind, U.: Five centuries of Stockholm winter/spring temperatures reconstructed from documentary evidence and instrumental observations, Climatic Change, 101, 109–141, 2010.

Linderholm, H. W. and Gunnarson, B. E.: Summer temperature variability in central Scandinavia during the last 3600 years, Geografiska Annaler: Series A, Phys. Geogr., 87, 231–241, https://doi.org/10.1111/j.0435-3676.2005.00255.x, 2005.

Linderholm, H. W., Björklund, J., Seftigen, K., Gunnarson, B. E., and Fuentes, M.: Fennoscandia revisited: a spatially improved tree-ring reconstruction of summer temperatures for the last 900 years, Clim. Dynam., 45, 933–947, 2015.

Lund, D. C., Lynch-Stieglitz, J., and Curry, W. B.: Gulf Stream density structure and transport during the past millennium, Nature, 444, 601–604, 2006.

Luterbacher, J., Werner, J. P., Smerdon, J. E., Fernández-Donado, L., González-Rouco, F. J., Barriopedro, D., and Esper, J.: European summer temperatures since Roman times, Environ. Res. Lett., 11, 024001, https://doi.org/10.1088/1748-9326/11/2/024001, 2016.

Mann, M. E. and Jones, P. D.: Global surface temperatures over the past two millennia, Geophys. Res. Lett., 30, https://doi.org/10.1029/2003GL017814, 2003.

Marchitto, T. M., Curry, W. B., Lynch-Stieglitz, J., Bryan, S. P., Cobb, K. M., and Lund, D. C.: Improved oxygen isotope temperature calibrations for cosmopolitan benthic foraminifera, Geochim. Cosmochim. Ac., 130, 1–11, 2014.

Masson-Delmotte, V., Schulz, M., Abe-Ouchi, A., Beer, J., Ganopolski, A., González Rouco, J. F., Jansen, E., Lambeck, K.,, Luterbacher, Naish, T., Osborn, T., Otto-Bliesner, B., Quinn, T., Ramesh, R., Rojas, M., Shao, X., and Timmermann, A.: Information from Paleoclimate Archives, in: Climate Change 2013: The Physical Science Basis, Contribution of Working Group I to the Fifth Assessment Report of the Intergovernmental Panel on Climate Change, edited by: Stocker, T. F., Qin, D., Plattner, G.-K., Tignor, M., Allen, S. K., Boschung, J., Nauels, A., Xia, Y., Bex, V., and Midgley, P. M., Cambridge University Press, Cambridge, United Kingdom and New York, NY, USA, 2013.

Mauquoy, D., van Geel, B., Blaauw, M., and van der Plicht, J.: Evidence from northwest European bogs shows "Little Ice Age" climatic changes driven by variations in solar activity, The Holocene, 12, 1–6, 2002.

Mayewski, P. A., Meeker, L. D., Twickler, M. S., Whitlow, S., Yang, Q. Z., Lyons, W. B., and Prentice, M.: Major features and forcing of high-latitude northern hemisphere atmospheric circulation using a 110,000-year-long glaciochemical series, J. Geophys. Res.-Ocean., 102, 26345–26366, 1997.

McCorkle, D. C., Corliss, B. H., and Farnham, C. A.: Vertical distributions and stable isotopic compositions of live (stained) benthic foraminifera from the North Carolina and California continental margins, Deep-Sea Res. Pt. I, 44, 983–1024, 1997.

McDermott, F., Mattey, D. P., and Hawkesworth, C.: Centennial-scale Holocene climate variability revealed by a high-resolution speleothem δ^{18}O record from SW Ireland, Science, 294, 1328–1331, 2001.

McGregor, H. V., Evans, M. N., Goosse, H., Leduc, G., Martrat, B., Addison, J. A., Mortyn, P. G., Oppo, D.W., Seidenkrantz, M.-S., Sicre, M.-A., Phipps, S. J., Selvaraj, K., Thirumalaj, K., Filipsson, H., and Ersek, V.: Robust global ocean cooling trend for the pre-industrial Common Era, Nat. Geosci., 8, 671–677, 2015.

Meeker, L. D. and Mayewski, P. A.: A 1400-year high-resolution record of atmospheric circulation over the North Atlantic and Asia, The Holocene, 12, 257–266, 2002.

Mikalsen, G., Sejrup, H. P., and Aarseth, I.: Late-Holocene changes in ocean circulation and climate: foraminiferal and isotopic evidence from Sulafjord, western Norway, The Holocene, 11, 437–446, 2001.

Miller, G. H., Geirsdottir, A., Zhong, Y. F., Larsen, D. J., Otto-Bliesner, B. L., Holland, M. M., Bailey, D. A., Refsnider, K. A., Lehman, S. J., Southon, J. R., Anderson, C., Bjornsson, H., and Thordarson, T.: Abrupt onset of the Little Ice Age triggered by volcanism and sustained by sea-ice/ocean feedbacks, Geophys. Res. Lett., 39, L02708, https://doi.org/10.1029/2011GL050168, 2012.

Millet, L., Arnaud, F., Heiri, O., Magny, M., Verneaux, V., and Desmet, M.: Late-Holocene summer temperature reconstruction from chironomid assemblages of Lake Anterne, northern French Alps, The Holocene, 19, 317–328, 2009.

Moberg, A., Sonechkin, D. M., Holmgren, K., Datsenko, N. M., and Karlén, W.: Highly variable Northern Hemisphere temperatures reconstructed from low- and high-resolution proxy data, Nature, 433, 613–617, 2005

Morris, C. D.: Viking Orkney: a survey, in: The Prehistory of Orkney, editedn by: Renfrew, C., Edinburgh University Press, Edinburgh, 1985.

Nardelli, M. P., Barras, C., Metzger, E., Mouret, A., Filipsson, H. L., Jorissen, F., and Geslin, E.: Experimental evidence for foraminiferal calcification under anoxia, Biogeosciences, 11, 4029–4038, https://doi.org/10.5194/bg-11-4029-2014, 2014.

Nordberg, K.: Oceanography in the Kattegat and Skagerrak over the past 8000 years, Paleoceanography, 6, 461–484, 1991

Nordberg, K., Gustafsson, M., and Krantz, A. L.: Decreasing oxygen concentrations in the Gullmar Fjord, Sweden, as confirmed by benthic foraminifera, and the possible association with NAO, J. Marine Syst., 23, 303–316, 2000.

Nordberg, K., Filipsson, H. L., Linné, P., and Gustafsson, M.: Stable isotope evidence for the recent establishment of a new, opportunistic foraminiferal fauna within Gullmar Fjord, Sweden, J. Mar. Micropal., 73, 117–128, 2009.

O'Neil, J. R., Clayton, R. N., and Mayeda, T. K.: Oxygen isotope fractionation in divalent metal carbonates, J. Chem. Phys., 51, 5547–5558, 1969.

Orme, L. C., Davies, S. J., and Duller, G. A. T.: Reconstructed centennial variability of late Holocene storminess from Cors Fochno, Wales, UK, J. Quaternary Sci., 30, 478–488, 2015.

Ortega, P., Montoya, M., González-Rouco, F., Mignot, J., and Legutke, S.: Variability of the Atlantic meridional overturning circulation in the last millennium and two IPCC scenarios, Clim. Dynam., 38, 1925–1947, 2012.

Orth, R., Vogel, M. M., Luterbacher, J., Pfister, C., and Seneviratne, S. I.: Did European temperatures in 1540 exceed present-day records?, Env. Res. Lett., 11, 114021, https://doi.org/10.1088/1748-9326/11/11/114021, 2016.

Otterå, O. H., Bentsen, M., Drange, H., and Suo, L.: External forcing as a metronome for Atlantic multidecadal variability, Nat. Geosci., 3, 688–694, 2010.

PAGES 2K Consortium: Continental scale temperature variability during the past two millennia, Nat. Geosci., 6, 339–982, 2013.

PAGES 2K Consortium: Data descriptor: A global multiproxy database for temperature reconstructions of the common era, Nature Scientific Data, 4, 170088, https://doi.org/10.1038/sdata.2017.88, 2017.

Park, W. and Latif, M.: Multidecadal and multicentennial variability of the meridional overturning circulation, Geophys. Res. Lett., 35, L22703, https://doi.org/10.1029/2008GL035779, 2008.

Pauling, A., Luterbacher, J., Casty, C., and Wanner, H.: 500 years of gridded high-resolution precipitation reconstructions over Europe and the connection to large-scale circulation, Clim. Dynam., 26, 387–405, 2006.

Perner, K., Moros, M., Lloyd, J. M., Jansen, E., and Stein, R.: Mid to late Holocene strengthening of the East Greenland Current linked to warm subsurface Atlantic water, Quaternary Sci. Rev., 129, 296–307, 2015.

Pettersson, O. and Ekman, G.: Grunddragen af Skageracks och Kattegats hydrografi, Kongl. Svenska Vetenskaps-akademiens handlingar, 24, 130 pp., 1891.

Polovodova, I., Nordberg, K., and Filipsson, H. L.: The benthic foraminiferal record of the Medieval Warm Period and the recent warming in the Gullmar Fjord, Swedish west coast, Mar. Micropaleontol., 81, 95–106, 2011.

Polovodova Asteman, I. and Nordberg, K.: Foraminiferal fauna from a deep basin in Gullmar Fjord: the influence of seasonal hypoxia and North Atlantic Oscillation, J. Sea Res., 79, 40–49, 2013.

Polovodova Asteman, I., Nordberg, K., and Filipsson, H. L.: The Little Ice Age: evidence from a sediment record in Gullmar Fjord, Swedish west coast, Biogeosciences, 10, 1275–1290, https://doi.org/10.5194/bg-10-1275-2013, 2013.

Poole, D. A. R., Dokken, T. M., Hald, M., and Polyak, L.: Stable isotope fractionation in recent benthic foraminifera from the Barents and Kara Seas, PhD, University of Bergen, 1994.

Porter, S. C.: Pattern and forcing of Northern-Hemisphere glacier variations during the last millenium, Quaternary Res., 26, 27–48, 1986.

Reimer, P. J., Baillie, M. G. L., Bard, E., Bayliss, A., Beck, J. W., Bertrand, C. J. H., Blackwell, P. G., Buck, C. E., Burr, G. S., Cutler, K. B., Damon, P. E., Edwards, R. L., Fairbanks, R. G., Friedrich, M., Guilderson, T. P., Hogg, A. G., Hughen, K. A., Kromer, B., McCormac, G., Manning, S., Ramsey, C. Bronk, Reimer, R. W., Remmele, S., Southon, J. R., Stuiver, M., Talamo, S., Taylor, F. W., van der Plicht, J., and Weyhenmeyer, C. E.: Int- Cal04 terrestrial radiocarbon age calibration, 0–26 cal kyr BP, Radiocarbon, 46, 1029–1058, 2004.

Reimer, P. J., Bard, E., Bayliss, A., Beck, J. W., Blackwell, P. G., Bronk Ramsey, C., Buck, C. E., Cheng, H., Edwards, R. L., Friedrich, M., Grootes, P. M., Guilderson, T. P., Haflidason, H., Hajdas, I., Hatté, C., Heaton, T. J., Hoffman, D. L., Hogg, A. G., Hughen, K. A., Kaiser, K. F., Kromer, B., Manning, S. W., Niu, M., Reimer, R. W., Richards, D. A., Scott, E. M., Southon, J. R., Staff, R. A., Turney, C. S. M., and van der Plicht, J.: Int Cal13 and Marine13 radiocarbon age calibration curves 0–50,000 years cal BP, Radiocarbon, 55, 1869–1887, 2013.

Reverdin, G.: North Atlantic subpolar gyre surface variability (1895–2009), J. Clim., 23, 4571–4584, 2010.

Reverdin, G., Cayan, D., Dooley, H. D., Ellett, D. J., Levitus, S., Du Penhoat, Y., and Dessier, A.: Surface salinity of the North Atlantic: can we reconstruct its fluctuations over the last one hundred years?, Prog. Oceanogr., 33, 303–346, 1994.

Richter, T. O., Peeters, F. J., and van Weering, T. C.: Late Holocene (0–2.4 kaBP) surface water temperature and salinity variability, Feni Drift, NE Atlantic Ocean, Quaternary Sci. Rev., 28, 1941–1955, 2009.

Risebrobakken, B., Dokken, T., Smedsrud, L. H., Andersson, C., Jansen, E., Moros, M., and Ivanova, E. V.: Early Holocene temperature variability in the Nordic Seas: The role of oceanic heat advection versus changes in orbital forcing, Paleoceanography, 26, PA4206, https://doi.org/10.1029/2011PA002117, 2011.

Rydberg, L.: Circulation in the Gullmaren – a silll fjord with externally maintained stratification. Inst. of Oceanography, Univ. of Gothenburg, Report no: 23 (mimeo), Gothenburg, 1977.

Salvesen, H.: Jord i Jämtland, Östersund, AB Wisenska bokhandelens förlag, 187 pp., 1979.

Schmittner, A., Latif, M., and Schneider, B.: Model projections of the North Atlantic thermohaline circulation for the 21st century accessed by observations, Geophys. Res. Lett., 32, L23710, https://doi.org/10.1029/2005GL024368, 2005.

Seidenkrantz, M. S., Aagaard-Sørensen, S., Sulsbrück, H., Kuijpers, A., Jensen, K. G., and Kunzendorf, H.: Hydrography and climate of the last 4400 years in a SW Greenland fjord: implications for Labrador Sea palaeoceanography, The Holocene, 17, 387–401, 2007.

Shackleton, N. J.: Attainment of isotopic equilibrium between ocean water and the benthonic foraminifera genus *Uvigerina*: isotopic changes in the ocean during the last glacial, Colloques Internationaux du CNRS nr. 219, 203–209, 1974.

Sicre, M. A., Hall, I. R., Mignot, J., Khodri, M., Ezat, U., Truong, M. X., Eiriksson, J., and Knudsen, K. L.: Sea surface temperature variability in the subpolar Atlantic over the last two millennia, Paleoceanography, 26, PA4218, https://doi.org/10.1029/2011PA00216, 2011.

Sicre, M.-A., Weckström, K., Seidenkrantz, M.-S., Kuijpers, A., Benetti, M., Masse, G., Ezat, M., Schmidt, S., Bouloubassi, I., Olsen, J., Khodri, M., and Mignot, J.: Labrador current variability over the last 2000 years, Earth Planet. Sc. Lett., 400, 26–32, 2014.

SMHI-SHARK database, https://www.smhi.se/klimatdata/oceanografi/havsmiljodata/marina-miljoovervakningsdata, last access: 15 March 2017.

SMHI: Meteorological observations of air temperatures, https://www.smhi.se/klimatdata, last access: 15 March 2017.

Stuiver, M. and Pollach, H. A.: Discussions of reporting ^{14}C data, Radiocarbon, 19, 355–363, 1977.

Stuiver, M., Grootes, P. M., and Braziunas, T. F.: The GISP2 δ^{18}O climate record of the past 16,500 years and the role of sun, ocean and volcanoes, Quaternary Res., 44, 341–354, 1995.

Stuiver, M., Reimer, P. J., and Reimer, R. W.: CALIB 7.1 [WWW program], available at: http://calib.org, last access: 16 February 2017.

Svansson A : Physical and chemical oceanography of the Skagerrak and the Kattegat, I. Open Sea Conditions, Institute of Marine Research, Report No. 1. Lysekil: Fishery Board of Sweden, 1–88, 1975.

Tarutani T., Clayton R. N., and Mayeda T. K.: The effect of polymorphism and magnesium substitution on oxygen isotope fractionation between calcium carbonate and water, Geochim. Cosmochim. Ac., 33, 987–996, 1969.

Thornalley, D. J., Elderfield, H., and McCave, I. N.: Holocene oscillations in temperature and salinity of the surface subpolar North Atlantic, Nature, 457, 711–714, 2009.

Thornalley, D. J. R., Oppo, D. W., Ortega, P., Robson, J. I., Brierley, C. M., Davis, R., Hall, I. P., Moffa-Sanchez, P., Rose, N. L., Spooner, P. T., Yashayaev, I., and Keigwin, L.: Anomalously weak Labrador Sea convection and Atlantic overturning during the past 150 years, Nature, 556, 227–232, 2018.

Trouet, V., Esper, J., Graham, N. E., Baker, A., Scourse, J. D., and Frank, D. C.: Persistent Positive North Atlantic Oscillation Mode Dominated the Medieval Climate Anomaly, Science, 324, 78–80, 2009.

Van der Schrier, G. and Barkmeijer, J.: Bjerknes hypothesis on the coldness during AD 1790–1820 revisited, Clim. Dynam., 25, 537–553, 2005.

Wagner, S. and Zorita, E.: The influence of volcanic, solar and CO_2 forcing on the temperatures in the Dalton minimum (1790–1830): a model study, Clim. Dynam., 25, 205–218, 2005.

Wang, T., Surge, D., and Mithen, S.: Seasonal temperature variability of the Neoglacial (3300–2500 BP) and Roman Warm Period (2500–1600 BP) reconstructed from oxygen isotope ratios of limpet shells (*Patella vulgata*), Northwest Scotland, Palaeogeogr. Palaeocl., 317/318, 104–113, 2012.

Wanner, H., Solomina, O., Grosjean, M., Ritz, S. P., and Jetel, M.: Structure and origin of Holocene cold events, Quaternary Sci. Rev., 30, 3109–3123, 2011.

Wetter, O., Pfister, C., Werner, J. P., Zorita, E., Wagner, S., Senevirante, S. I., Herget, J., Grünewald, U., Luterbacher, J., Alcoforado, M.-J., Barriendos, M., Bieber, U., Brázdil, R., Burmeister, K. H., Camenish, S., Contino, A., Dobrovolny, P., Glaser, R., Himmelsbach, I., Kiss, A., Kotyza, O., Labbe, T., Limanowka, D., Litzenburger, L., Nordl, Ø., Pribyl, K., Retsö, D., Riemann, D., Rohr, C., Siegfried, W., et al.: The year-long unprecedented European heat and drought of 1540 – a worst case, Climatic Change, 125, 349–63, 2014.

Zicheng, Y. and Ito, E.: Historical solar variability and midcontinent drought, Pages Newsl., 8, 6–7, 2000.